Graphene edge chemistry and membrane formation with supramolecular approaches using Pt(II)-terpyridine molecular tweezers

Jiao, A.

CHAPTER 1

Introduction

1.1 General context

Current DNA sequencing technologies often use biological nanopores, which are proteins with nanometer-scale holes that form a channel through a membrane, for example, a lipid bilayer.[1] While these nanopores possess a precisely defined chemical structure, their nanometer thickness limits the resolution of DNA sequencing to the detection of no fewer than three nucleotides at once.[2] By decreasing the thickness of the nanopore down to the thickness of a single atom, the theoretical limit of spatial resolution can be reached. This apparently simple concept requires the use of solid-state nanopores made using two-dimensional (2D) materials, such as graphene.[3,4] However, compared to biological nanopores,[1] the chemical structure around the edges of graphene nanopores is often poorly defined. This ambiguity includes different possible termination groups for graphene edges,[5] contamination originating from fabrication techniques,[6] or side reactions during covalent functionalization such as diazotization.[7] To obtain chemically defined graphene edges, non-covalent functionalization can be employed with well-defined molecules that can target the edges. One method would be using molecular tweezers, which are U-shaped molecules with a cavity for binding substrates,[8] to selectively functionalize graphene nanopore edges. The structure of these molecular tweezers can be adjusted to introduce additional functionality at the graphene edges, such as molecular recognition (base pairings) or spectroscopic enhancement (nanoparticles, fluorescent probes, etc.). Being able to control the chemical functionality of graphene edges is anticipated to enable new techniques in nanopore sequencing.

To reliably obtain defined graphene edges using molecular tweezers, it is vital to attain a fundamental understanding of the binding behavior between the tweezers and their substrate. Direct characterization of graphene edges is challenging, as it requires high-end instrumentation and techniques capable of achieving atomic resolution. On the other hand, these instruments often operate under high-vacuum conditions that are incompatible with solution self-assembly.[5] Therefore, molecules such as polycyclic aromatic hydrocarbons (PAHs) can serve as models for graphene.[9] Unlike graphene, PAHs are soluble and can be characterized appropriately by using solution-based techniques (NMR, UV/Vis, etc.) that are routinely available in chemistry labs. These techniques enable efficient characterization of the influence of different components, including the structure of molecular tweezers, the PAH, and the solvent environment. The obtained information can later be integrated into the functionalization of real graphene nanopore devices. This introductory chapter describes the history of DNA sequencing that led to the development of nanopore technology, as well as

background information on molecular tweezers and PAHs to set the context for their implementation in graphene nanopore devices.

1.2 History of DNA sequencing

Deoxyribonucleic acid (DNA) is a biopolymer consisting of two complementary polynucleotide chains, each composed of four nucleotides: adenine (A), thymine (T), cytosine (C) and guanine (G). The exact sequence of these nucleotides serves as the genetic blueprint of an organism, influencing its identity, physiology, and other biological traits. Therefore, the ability to decipher the sequence of DNA has greatly advanced many fields of biology, including medical diagnosis, forensic sciences, agriculture and biotechnology.[10] The sequencing technology has undergone a remarkable evolution since the discovery of DNA (Figure 1.1). In 1953, almost a century after the discovery of DNA (initially named "nuclein") by Friedrich Miescher in 1869,[11,12] the combined efforts of Watson, Crick, Wilkins and Franklin revealed that DNA is an antiparallel double helix comprised of four different nucleotides.[13,14] After this discovery, research on DNA sequencing was on the rise. In 1972, Jou et al. produced the first nucleotide sequence of a gene, which encoded the coat protein of Bacteriophage MS2.[15] This sequence was solved using identified DNA fragments obtained from selective DNA fragmentation combined with analytical chemistry to determine the oligonucleotide composition.[16,17] Later in 1977, Sanger et al. invented a groundbreaking method of DNA sequencing, which is now known as Sanger sequencing.[18]

Sanger sequencing is one of the first-generation sequencing techniques. It is based on the chain-termination method, which uses radioactively or fluorescently labeled dideoxynucleotide triphosphate (ddNTP) variants of each nucleotide (ddATP, ddTTP, ddCTP and ddGTP) to terminate DNA strand elongation to obtain fragmented DNA strands of various lengths.[19] The different sizes of DNA can then be visualized after gel electrophoresis, from which the terminating nucleotide can be inferred from the distance travelled in the gel.[20] Many improvements were made over the following years. Polymerase chain reaction (PCR) allowed rapid DNA amplification.[21,22] The 'shotgun sequencing' technique used many short overlapping DNA fragments to solve longer DNA sequences.[23,24] Development of automation techniques continued to increase the scale of DNA sequencing to millions of base pairs per year.[25] The combination of many optimization technologies has made sequencing of the first human genome possible, marking the end of the Human Genome Project (HGP) in 2003.[26] Despite these achievements, first-generation DNA sequencing techniques remained laborious and poorly scalable.

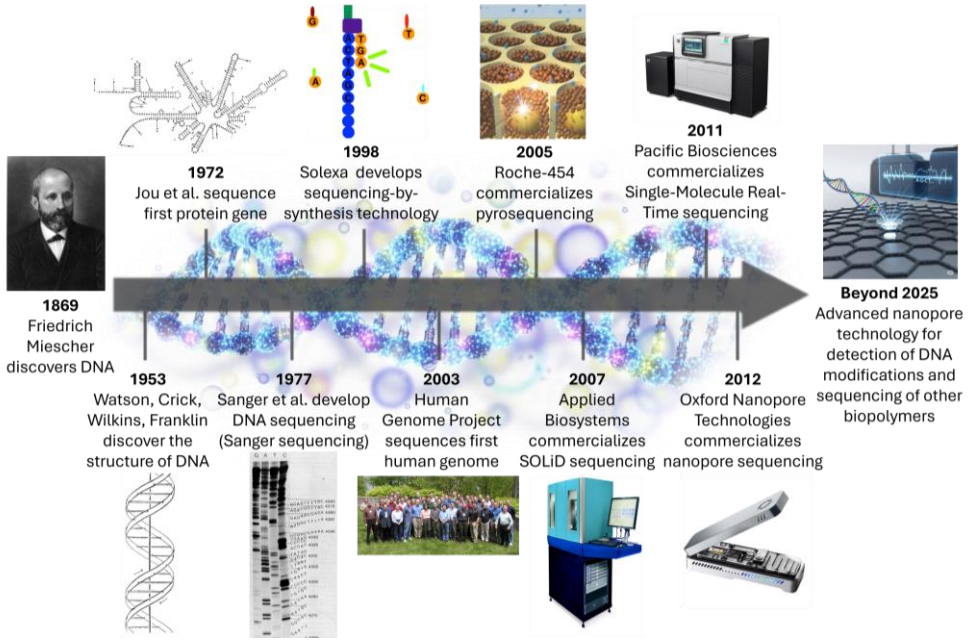

Figure 1.1 Timeline highlighting some of the notable accomplishments in the history of DNA sequencing. The timeline is not scaled proportionally.

In the following decades, a lot of research was aimed at making DNA sequencing scalable, which is the hallmark of second-generation DNA sequencing. Several platforms have been developed, such as 454 pyrosequencing by Roche,[27] SOLiD (Supported Oligonucleotide Ligation and Detection) by Applied Biosystems,[28] Ion Torrent (ion semiconduction sequencing) by Life Technologies,[29] and sequencing-by-synthesis by Solexa (later acquired by Illumina),[30] with the latter still being one of the main sequencing platforms to date.[31] Thus, Solexa/Illumina sequences DNA by measuring distinct fluorescent signals depending on the nucleotide that is being incorporated during DNA synthesis.[32] This method requires a large amount of DNA and immobilization of DNA to distinguish different DNA fragments, which is made possible by growing clusters of DNA on surfaces using solid-phase PCR.[33] As a result, the sequencing of many different DNA fragments can be performed in parallel, greatly speeding up the process. However, the downside is that only small fragments of DNA (up to several hundred base pairs) can be read, as longer DNA strands are more difficult to amplify efficiently and can lower readout accuracy and resolution due to the accumulation of side reactions. The limitation to short DNA fragments complicates the reconstruction of complete genomes and is unsuitable for analyzing complex samples,[34] such as detecting viral DNA within the human microbiome.

To overcome the limitations of second-generation sequencing techniques, platforms were developed to sequence longer fragments or entire strands of DNA, now known as third-generation DNA sequencing. These platforms focused on eliminating the need for DNA amplification and enabling real-time DNA sequencing. Next to single-molecule real-time (SMRT) sequencing technology pioneered by Pacific Biosciences (PacBio),[35] the most anticipated platform for single-molecule sequencing is nanopore sequencing pioneered by Oxford Nanopore Technology (ONT).[36] Nanopore sequencing technology uses single pores at the nanometer scale embedded in membranes dividing two chambers.[37] The chambers can be filled with electrolyte solution and molecules of interest, such as DNA. Upon applying an electric field across this membrane, the electrolyte and DNA will flow through the nanopore, resulting in a measurable ionic current (Figure 1.2A). The magnitude of the ionic current is dependent on the size of the nanopore as well as the obstruction of the nanopore, such as any traversing DNA. This blockage will lead to different levels of ionic current depending on which nucleotides are blocking the pore, which can be used to differentiate nucleotides during DNA sequencing. The identification of molecules or particles through variations in the ionic current is called the Coulter principle.[38] Though the accuracy of third-generation sequencing is lower than for second-generation sequencing, the time to complete the sequencing of the human genome can be decreased by orders of magnitude with the added advantage of also reading longer DNA fragments (read lengths on the order of 10^2 vs. 10^5 base pairs for second-generation vs. third-generation sequencing techniques, respectively).[39,40]

State-of-the-art nanopore sequencing devices are based on biological nanopores embedded in a lipid bilayer.[41] For example, α-Hemolysin (α-HL)[42,43] and *Mycobacterium smegmatis* porin A (MspA)[44,45] are biological nanopores with relevant pore sizes to enable detectable changes in ionic current during single-stranded DNA (ssDNA) translocation.[46–48] However, the average dwell time during ssDNA electrophoresis through bare biological pores is ~1 – 20 μs per nucleotide (at 120 mV bias).[49,50] At these fast rates, the nucleic acid sequence cannot be accurately obtained by nanopore detecting instruments.[50,51] To slow down DNA translocation, biological nanopores were paired with a motor protein called Phi29 DNA polymerase to ratchet DNA through the nanopore at a controlled speed, allowing dwell times to reach >3 ms per nucleotide.[52,53] The use of this motor protein, amongst others,[54–57] was key to enabling DNA sequencing using nanopore technology. Now, biological nanopore devices can read sequences of up to several million base pairs in length[58,59] and have the ability to distinguish base modifications such as methylation without the need for additional experimental preparation.[60,61]

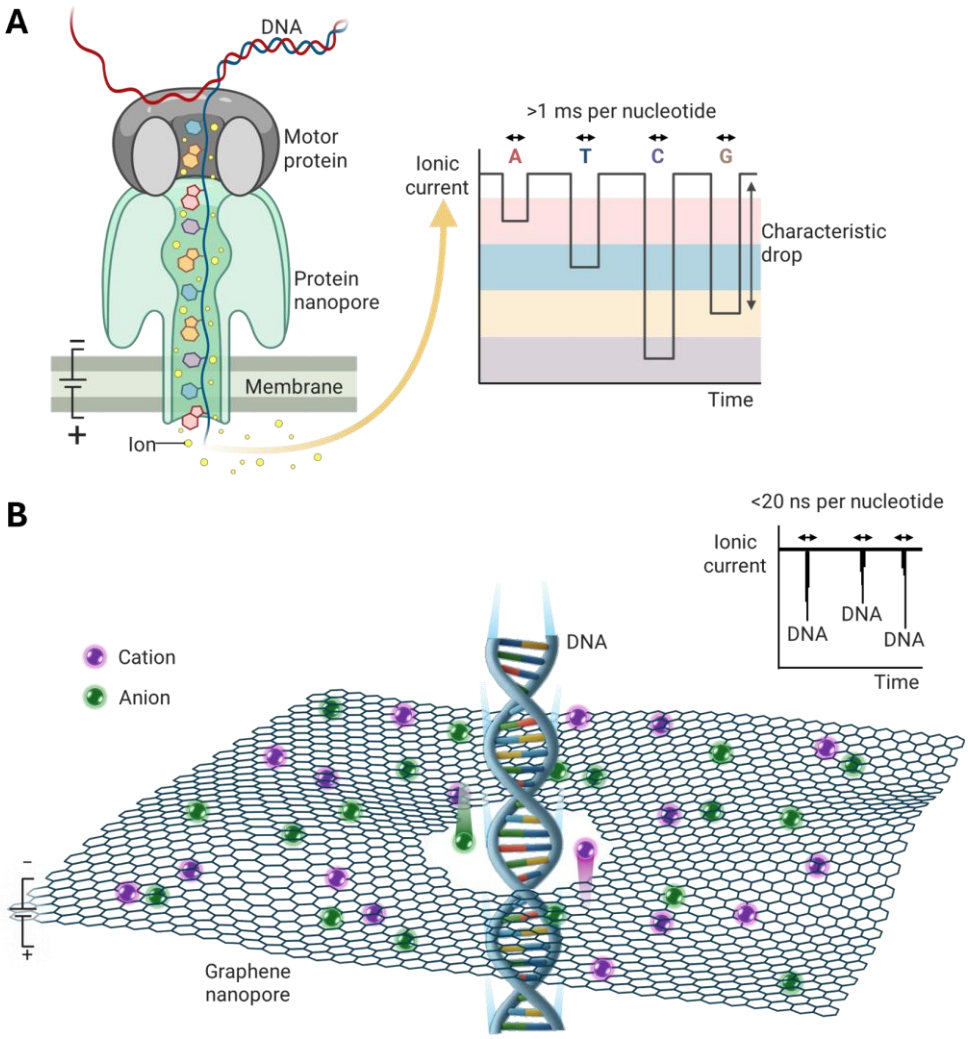

Figure 1.2 Illustration of DNA sequencing using biological and graphene nanopores. (A) As the motor protein unwinds the double-stranded DNA (dsDNA), one of the strands is threaded through the pore towards the positive side of the membrane. In an ideal case, as each nucleotide passes through the pore, a characteristic drop in ionic current is measured depending on the translocating base, enabling sequencing of the DNA. Figure was made with BioRender (original created by Flo Glencross and Daid Ahmad Khan).[62] (B) Upon applying an electric field over a graphene nanopore membrane, the DNA and electrolyte in solution rapidly move through the pore, generating a measurable ionic current. In the case of bare graphene nanopores, when DNA strands translocate through the nanopore, current blockages in the form of abrupt spikes are observed for the passage of entire DNA strands, corresponding to short dwell times of generally <20 ns per nucleotide.[63–65] Figure was made with BioRender.

1.3 Advanced materials for nanopore technology

Ever since the success of biological nanopores, interest has grown in fabricating solid-state nanopores composed of non-biological materials. Compared to biological nanopores, solid-state nanopores offer, in theory, many advantages, including improved stability, adaptability to longer or more variations in operating conditions, higher flexibility in fabrication and integration techniques, and better customizability for a wider range of applications.[66] These properties are especially important when considering to apply nanopore technology beyond DNA sequencing.[67] A wide variety of materials, especially materials compatible with semiconductor fabrication techniques,[68] have shown potential as solid-state nanopores for DNA sensing, including silicon nitride (SiN_x),[69] silicon dioxide (SiO_2),[70] and more.[71–74] Additionally, many solid-state nanopores have been demonstrated to be useful for protein sensing[75,76] and characterization.[77,78] Ideally, nanopores would be employed to enable real-time sequencing by translating detectable changes, *e.g.* ionic current, into recognition of individual building blocks, *e.g.* nucleic acids or amino acids. One particular advantage of solid-state nanopores over biological nanopores is that they provide, in principle, greater control over their pore dimensions.

The thickness of the nanopore determines its spatial resolution. Ideally, individual building blocks could be identified from changes in ionic current during translocation. In the case of DNA, this would be four distinct ionic current blockades corresponding to the four different nucleotides. However, state-of-the-art protein nanopores are thicker (≥1.6 nm in length at the sensing region,[79] and ~5 nm total protein lengths)[80] than the spacing between the nucleotides in the DNA (0.34 nm).[13,81] Consequently, a multitude of current changes are observed stemming from the many different nucleotide combinations. Therefore, minimizing the thickness of nanopores is key to improving the accuracy of DNA sequencing. The thickness is especially important when considering biomolecules with even smaller building blocks, like amino acids in proteins. Combined with the fact that there are 20 different standard amino acids and over 400 possible post-translational modifications,[82] the high number of different current changes adds further complexity to the deconvolution of protein sequences.

To increase the spatial resolution in nanopore sequencing, many efforts have been made to produce nanopores in two-dimensional (2D) materials. One of the most promising 2D materials is graphene, a single layer of carbon atoms arranged in a hexagonal lattice. After its discovery in 2004 by Geim and Novoselov et al.,[83] it is argued that its atomic-scale thickness provides the ultimate sensitivity for

distinguishing single building blocks, such as nucleotides, during translocation. Successful translocation of double-stranded DNA (dsDNA) through graphene nanopores has been demonstrated since 2010 (Figure 1.2B).[63–65] Since then, DNA translocation has been tested in other 2D materials as well, such as boron nitride (BN),[84] molybdenum sulfide (MoS_2),[85] and 2D transition metal carbides (2D TMCs, also known as MXenes).[86] Although atomic-scale thickness would be ideal, the disadvantage is a decreased temporal resolution because of the high translocation speed through graphene nanopores. With dwell times less than 1 μs per nucleotide in these devices,[87] insufficient data points can be obtained per translocating nucleotide with existing data acquisition instruments for accurate DNA sequencing. While it would be ideal to combine the motor proteins like phi29 with solid-state nanopores, proteins tend to stick to the surfaces of solid-state nanopores,[88,89] which leads to frequent clogging of the nanopores and loss of protein function.[90] Therefore, other avenues of slowing down translocation speed have been explored.

To slow down DNA translocation speed in solid-state nanopores, researchers have investigated many parameters,[91] including nanopore size,[92,93] bias voltage,[92,94] temperature,[92,95] viscosity,[96,97] surface charge,[98–101] and electrolyte concentration[102,103] and composition.[104] Reducing the voltage bias can decrease the driving force and speed of DNA translocation, though at the cost of reducing the signal-to-noise (SNR) ratio.[92,94] Decreasing the pore size can increase friction, which in turn slows down DNA translocation.[92,93] Lowering the temperature[92,95] and increasing the solvent viscosity[96,97] can increase the drag force on DNA, also slowing down DNA translocation. For example, replacing the chloride anion for glutamate, which acts as a thickening agent, slowed down translocation speeds by up to 11 times.[97] However, glutamate solutions also present other complications, such as reduced solubility. Instead of the anion, the cation can also be changed. For example, Li^+ can bind more strongly to DNA than K^+, which decreases the effective charge of DNA and hence slows down its translocation.[104] Additionally, coating the pore surface with positively charged species such as adsorbed Ca^{2+} can slow down DNA translocation by almost two orders of magnitude through additional electrostatic interactions.[100] Alternatively, coating pore surfaces with negatively charged sodium dodecyl sulfate can counteract DNA translocation through electro-osmotic flow (EOF), resulting in decreased translocation speeds up to 30-fold.[98] However, the EOF can also lead to repulsion of analytes, reducing their capture rates.[105] Ultimately, changing these mentioned parameters individually has not been demonstrated to slow down DNA translocation enough for efficient sequencing in solid-state nanopores. However, optimization of these environmental parameters,

such temperature and electrolyte concentration, can be combined with mechanical techniques to control DNA translocation speeds in the future.

Mechanical techniques to control DNA translocation include using a dual nanopore system,[106] optical trapping,[107] magnetic trapping,[108] plasmonic trapping,[109,110] and scanning probe immobilization,[111–113] among many others.[91,114] For example, by fabricating a device with two nanopores in close proximity, DNA can pass through both pores simultaneously, resulting in a "tug-of-war" scenario on the DNA between the two nanopores (Figure 1.3A).[106] However, such double-capture events are rare and lead to complex base identification reflected by ionic current blockages of two pores rather than one. Optical trapping employs dielectric particles whose position can be controlled and monitored in three dimensions using light (Figure 1.3B).[115] When DNA is tethered to these particles, the electrophoretic force on DNA can be counteracted by the optical force on the particle, resulting in reduced translocation speed.[107] Similarly, magnetic trapping employs DNA-tethered magnetic beads captured in magnetic field gradients (Figure 1.3C).[108] This technique can capture hundreds of beads simultaneously, enabling parallelization of DNA trapping and translocation, though it sacrifices some spatial control in three dimensions compared to optical trapping.[114] Importantly, both optical and magnetic trapping techniques lack nm-level spatial control of the beads because of Brownian motion.[112] Plasmonic trapping employs plasmonic nanostructures near the pore, which allows control over the nanopore resistance and ion flow upon light irradiation (Figure 1.3D).[116] This control can be used to slow down DNA translocation directly and is not limited by the particle size and material of the beads required in optical or magnetic trapping, where diffraction limits and strong light absorption or scattering pose problems.[117] However, plasmonic trapping suffers from fundamental difficulties such as interference of the ionic current and noise as a result from laser heating.[118] Alternatively, DNA can be mechanically immobilized onto a scanning probe in specialized systems that offer sub-nm spatial control, such as Atomic Force Microscopy (AFM) (Figure 1.3E).[111] Indeed, such techniques have reported to reach dwell times of more than 100 μs per nucleotide,[112] which are sufficient for nanopore-based DNA sequencing. However, fluctuations of the DNA in the pore complicate the sequencing readout in DNA-tethering systems,[119] which have thus far limited their use beyond discrimination of homopolymers.[113] Moreover, the experimental complexity and cost hinder their widespread application in research and development.

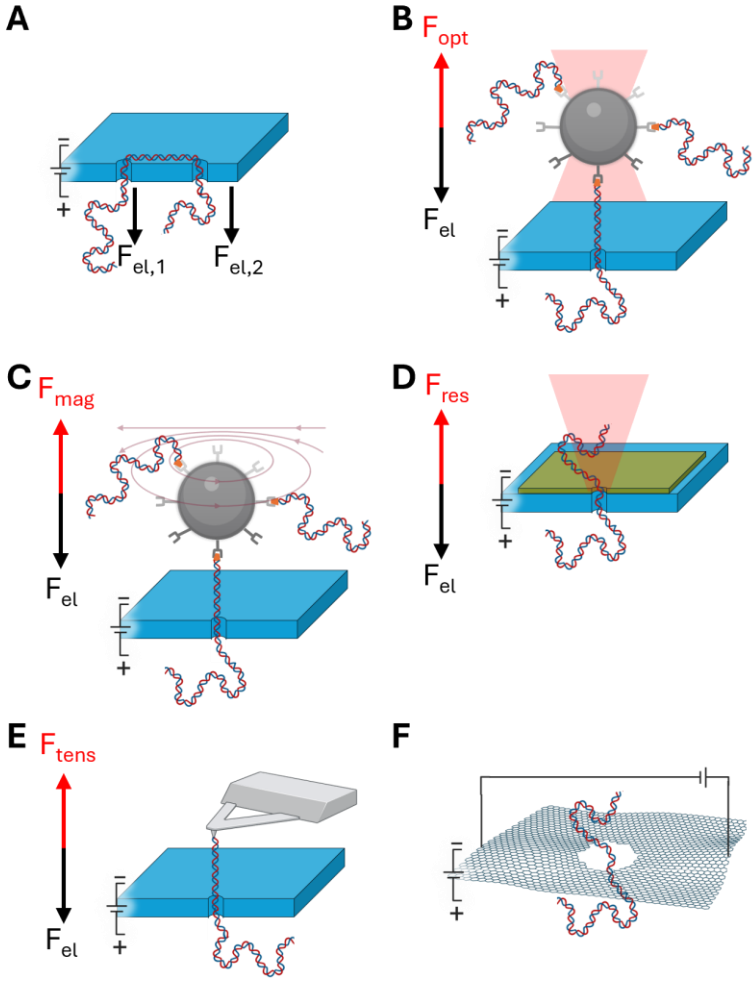

Figure 1.3 Illustrations of mechanical techniques to control and characterize DNA translocation in solid-state nanopores upon applying an electric field (F_{el}). (A) Dual nanopore systems produce a "tug-of-war" competition within the DNA strand when it is captured by both pores. (B) Optical trapping utilizes optical forces (F_{opt}) on the DNA-tethered dielectric beads to control their position. (C) Magnetic trapping utilizes magnetic forces (F_{mag}) on DNA-tethered magnetic beads to control their position. (D) Plasmonic trapping utilizes plasmonic nanostructures near the pore to manipulate the nanopore resistance (F_{res}) to slow down DNA translocation. (E) Scanning probe immobilization employs a sharp tip on a cantilever to mechanically control the tethered DNA translocation, which also generates a tension (F_{tens}) and vibrational signals that can be probed. (F) Transverse current application can be applied on conductive graphene membranes, generating a transverse electric field and a transverse current lateral to the ionic current. Consequently, an overall dragging force (F_{drag}) slows down DNA translocation. Figure was made with BioRender.

In addition to ionic current measurements to read the DNA sequence, alternative measurement techniques are actively being explored to be integrated in solid-state nanopores,[91,120] including fluorescence spectroscopy,[121] surface-enhanced Raman spectroscopy (SERS),[110] mechanical signaling,[112] and transverse current detection.[122,123] For example, fluorescence spectroscopy has been employed to detect the translocation of different single nucleotides in nanopore arrays.[124,125] Further improvements in fluorescence background elimination and target fluorescence enhancement are encouraging.[121] However, the downside of using fluorescence spectroscopy in nanopore-based sequencing is that the DNA needs to be labeled, which demands additional experimental preparation and can interfere with the ionic current readout. SERS does not require labeling of DNA and, through molecular dynamics simulations, has been demonstrated to enable DNA sequencing in tandem with plasmonic trapping (Figure 1.3D).[110] However, experimental evidence of SERS-based sequencing has not yet been reported. Additionally, trapping techniques can detect changes in mechanical forces such as probe position and vibrational amplitude during DNA translocation, which can provide additional signals for DNA sequencing (Figure 1.3E).[112] Next to these, a particularly promising sequencing technique is the transverse current detection proposed since 2005,[126–128] which is highly compatible with 2D materials. For instance, the high conductivity of graphene allows measuring of a current through the graphene sheet itself. Similar to the ionic current, this transverse current can be used to detect DNA translocation through graphene nanopores (Figure 1.3F).[129] The difference is that changes in ionic current depend on the geometry of the nucleotide residing in the pore, while the changes in transverse current depend on its electronic structure,[130] which is potentially advantageous for nanopore sequencing.[131] Indeed, an example advantage of increased signal-to-noise ratio has been demonstrated in MoS_2 nanopores.[123] However, the transverse current signals are difficult to separate from the ionic current signals due to capacitive coupling between the two channels, resulting in cross-talk.[132] Additionally, such complex devices face challenges in fabrication and reproducibility.[87]

1.4 Graphene nanopore fabrication and edge functionalization

Despite all the major developments in solid-state nanopores for DNA sequencing, a common problem remains the reliable fabrication of such devices, which are becoming increasingly complex as the field advances. Here, graphene nanopores are recognized as promising devices for DNA sequencing due to graphene's exceptional mechanical stability,[133,134] thermal and electrical conductivity,[135,136] and single atom

thickness.[137–139] One particularly challenging problem is controlling the edge chemistry of graphene, both during fabrication and after functionalization.

Graphene nanopores can be fabricated by various sculpting and etching techniques, including electron beam drilling,[140] focused ion beam etching,[141,142] plasma etching,[143] and controlled breakdown technique.[144] Electron beam drilling, also known as TEM drilling, uses high-energy electrons in transmission electron microscopy (TEM) to eject atoms from the material and create nanopores.[140] While this method offers high spatial control and *in situ* visualization of the pore, it is also prone to graphene damage and hydrocarbon contamination.[140,145,146] Focused ion beam (FIB) etching uses high-energy ions, for example gallium[142] and helium ion beams,[141] to fabricate nanopores. In contrast to TEM drilling, FIB etching is easier to scale through simultaneous sample processing,[147] though the cost of instrumentation remains relatively high. Plasma etching is significantly less demanding in terms of cost and complexity for large-scale graphene nanopore fabrication, however the disadvantage is little control over the position and size of the grown pores.[143] Moreover, plasma treatment can also introduce doping and defects in graphene, which can compromise its mechanical stability.[143] Therefore, controlled breakdown is being developed as a cost-effective nanopore fabrication technique with minimal surface contamination and introduction of defects. Controlled breakdown (CBD) is based on the dielectric breakdown technique, which employs a large electric field across a dielectric membrane in an electrolyte solution to accumulate charge traps and defects until the membrane breaks down to facilitate a conductive pathway.[144] This process can be controlled through careful voltage application combined with monitoring of the current to fabricate single nanopores with sub-nm precision in graphene.[148] However, downside of CBD is the poor control over the position of the obtained nanopores, as well as possible multiple pore creation.[149] Overall, each fabrication technique has its own advantages and disadvantages in terms of cost, scalability, and control over the nanopore size, position, and edge chemistry.[139,150,151]

To exert some control over the edge chemistry of graphene, several techniques have been developed to functionalize the graphene edges during or after fabrication.[5] For example, plasma treatment in the presence of H_2, O_2, or NH_3 can be used to functionalize graphene edges with hydrogen,[152,153] oxygen (*e.g.* ketones, ethers),[153,154] or nitrogen species (*e.g.* amines, imines), respectively (Figure 1.4a).[155–157] Alternatively, the graphene edges can be decorated with aryl-groups through free radical reaction with benzodiazonium salts (Figure 1.4b).[158,159] Although the graphene edge is generally more reactive than the basal plane,[5] the overwhelming

abundance of the basal plane relative to the edge often results in undesirable side reactions on the basal plane during plasma treatment and covalent organic reactions. Edge selectivity can be forced, for example, through the protection of the basal plane with a polymer film combined with the electrografting of the exposed edge with benzodiazonium salts.[160] However, polymer residues are difficult to remove completely from the basal plane,[6,161] and incomplete removal can lead to undesirable properties, such as compromised charge carrier mobility or thermal conductivity.[6,162] Another approach to selective edge functionalization could be utilizing the reactivity of newly created edges during controlled breakdown (CBD). The chemistry of graphene nanopores fabricated by CBD is likely dependent on the electrolyte solution, as electrolyte-dependent wall properties have been demonstrated in SiN_x nanopores.[100,101] However, since the CBD technique is restricted to current measurements, graphene nanopores fabricated by CBD rely on other techniques for *ex situ* characterization of their position, geometry and edge chemistry.

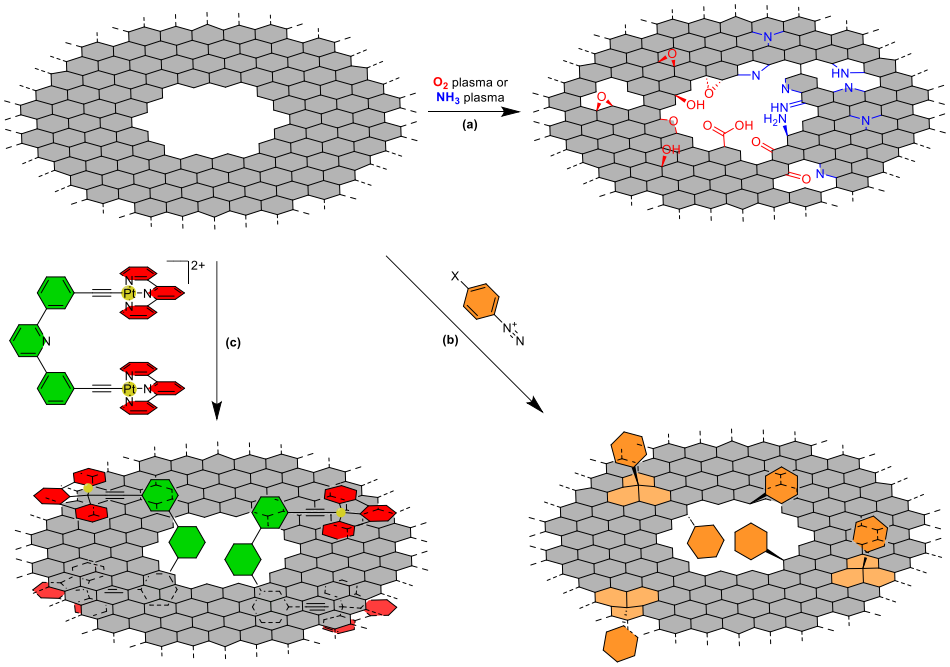

Figure 1.4 Schematic representation of graphene edge functionalization methods. (a) Plasma treatment with O_2 or NH_3 can be used to functionalize the graphene edges with oxygen and nitrogen species, respectively, along with basal plane functionalization and generation of vacancy defects. (b) Covalent functionalization using aryl-diazonium chemistry introduces aryl groups on both the basal plane and graphene edge. (c) Non-covalent functionalization using Pt(II)-terpyridine molecular tweezers can achieve edge-selective functionalization of the graphene without defect generation on the basal plane.

Few spectroscopic and microscopic techniques can distinguish the edge chemistry from that of the basal plane, which is a major obstacle in the pursuit of chemically defined graphene edges. Raman spectroscopy is commonly used to characterize the edge reactivity[159,163,164] or the density of introduced defects[165,166] (among other graphene properties such as doping or strain),[167] however it is unable to identify the exact chemical composition. X-ray photoelectron spectroscopy (XPS) can identify the exact chemical composition. However, its resolution is limited by its laser spot size, which is generally in the order of micrometers.[168] Transmission electron microscopy (TEM) can reach atomic resolution[169] and can be combined with spectroscopic techniques such as energy-dispersive x-ray (EDX) spectroscopy or electron energy-loss spectroscopy (EELS) to differentiate elements.[170,171] However, electron microscopy techniques are relatively invasive due to potential sample damage and contamination.[140,145,146] Scanning tunneling microscopy (STM) can also offer atomic resolution,[172,173] but its difficult operation combined with ultraclean sample requirements diminishes its practical applicability.

To visualize graphene edges on the nanometer scale with routinely available techniques such as scanning electron microscopy (SEM), the thiol-functionalized edges can be decorated with large Au nanoparticles through Au-S bond formation.[174,175] Such materials possess interesting electrocatalytic properties and the presence of nanoparticles can allow additional characterization using surface-enhanced Raman spectroscopy (SERS).[174,175] However, some Au nanoparticles were also observed on the basal plane, suggesting that these functionalization techniques could still target the basal plane and introduce defects.[174,175] Therefore, new edge-functionalization methods are needed to ensure preservation of the basal plane. Defect generation can be avoided by using non-covalent graphene functionalization instead, which does not rely on altering the chemical structure of graphene. Most non-covalent graphene functionalization strategies exploit its aromatic structure, which can provide strong π-π interactions among other interactions such as van der Waals, cation-π, *etc*.[176,177] However, these approaches generally focus on functionalization of the basal plane rather than the edges. Achieving edge-specific functionalization would require molecules capable of differentiating a flat surface from its edge. One possible avenue to accomplish this non-covalent selective graphene edge functionalization is through the use of molecular tweezers, which possess a cavity for the binding of substrates through non-covalent interactions (Figure 1.4c).

1.5 Molecular tweezers

Molecular tweezers fall within the scope of supramolecular chemistry, which describes the association between two or more molecules through non-covalent interactions, including van der Waals interactions, hydrogen bonding, electrostatic effects and π-π stacking forces.[178] A key element in supramolecular chemistry is the concept of host-guest chemistry,[179] where a host molecule selectively binds a guest molecule through complementary structural features. Among a wide variety of host molecules, molecular tweezers are a unique class of host molecules characterized by a backbone component connecting two "arms" (Figure 1.5).[8] In contrast to macrocyclic hosts with closed cavities, such as crown ethers and cryptands,[180–183] molecular tweezers contain a U-shaped cavity, resembling the shape of a pair of tweezers. Selectivity and properties of molecular tweezers are determined by their chemical structure. The spacer dictates the geometry and width of the binding cavity, whereas the recognition arms dictate the types of non-covalent interaction with the guest molecule. This design allows molecular tweezers to "tweeze" or clamp specific substrates. Furthermore, the tweezers' structure can be modified with functional features, such as photosensitization,[184] luminescence,[185] self-recognition,[186] and ion recognition,[187] to name just a few. These features make molecular tweezers powerful tools for various applications, including catalysis,[188,189] molecular recognition,[190] material science,[191,192] and pharmaceutical applications.[193]

The concept of molecular tweezers was first introduced by Chen and Whitlock in 1978.[194] They demonstrated that by connecting two caffeine moieties as the arms with a rigid diyne backbone, self-association of the two caffeine arms was prevented (Figure 1.5). The distance between the two arms formed a cavity of ~7 Å, which is optimal for π-π stacking interactions,[195] allowing the complexation of other theophylline derivatives.[194] Molecular tweezers started to gain more traction at the end of the 20th century.[8] Around this time, researchers were exploring the field of host-guest chemistry to study and mimic biological processes, a movement pioneered by Donald J. Cram and Jean-Marie Lehn.[178,196] Similar to the first defined molecular tweezer by Chen and Whitlock,[194] early examples of molecular tweezers often feature rigid backbones and aromatic arms to exploit preorganization and π-π stacking interactions.[8] Subsequent research expanded structural diversity to improve solubility, which can be achieved, for example, by attaching anionic phosphonate, phosphate, or sulfate functional groups to the chemical structure.[188] Additionally, conformational switching can be achieved by adding stimuli-responsive moieties in flexible backbones, for example, bipyridine or terpyridine backbones can participate

in metal chelation and alter the tweezers conformation depending on the substitution pattern.[197–200]

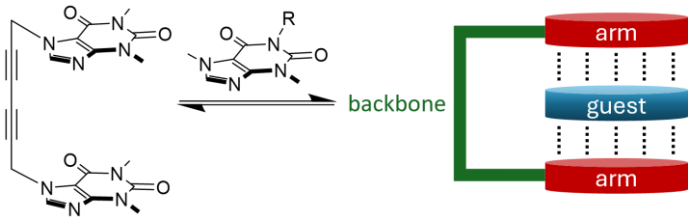

Figure 1.5 The first molecular tweezers and their concept of binding. The first molecular tweezers were composed of two caffeine moieties as the arms and a diyne moiety as the backbone.[194] These molecular tweezers contain a binding cavity between the arms that can host other theophylline derivatives as guest molecules through non-covalent interactions.

Molecular tweezers have received a lot of attention for their selective binding of guests such as ions,[187] amino acids,[201] and nucleic acids,[202,203] which have been exceptionally promising in biological applications.[193] Particularly, Fokkens et al.[201] developed water-soluble molecular tweezers with an apolar cavity and phosphonate groups that can selectively bind lysine or arginine.[201] Multivalent versions of these tweezers were demonstrated to act as inhibitors of p97 enzymes by blocking the entry of the enzyme's pore.[204] Additionally, such tweezers can bind lysine and arginine in amyloid beta (Aβ) peptides and subsequently inhibit Aβ oligomerization and aggregation,[205] which plays a role in neurodegenerative diseases such as Alzheimer's disease.[206] These tweezers have been tested in mice to successfully mitigate pathological protein aggregation.[207,208]

A distinct type of molecular tweezers were developed with the focus on binding planar guests such as polycyclic aromatic hydrocarbons (PAHs) and organometallic complexes (OMCs).[190,209] Several of these tweezers are a combination of substructures as given in Figure 1.6, and a list of their reported guests and association constants is given in Table 1.1. These tweezers often incorporate aromatic organometallic arms like **1**, **2** and **3** to facilitate π-π and metal-metal interactions, affording association constants reaching the order of 10^5 M^{-1} and allowing complexation to occur at micromolar concentrations.[184] In addition to these interactions, charge-transfer interactions arising from electron-rich donor and electron-poor acceptor moieties play a crucial role.[191] For instance, electron-rich arms **4** strongly bind electron-deficient guests such as nitro-substituted PAHs.[210] Conversely, electron-rich guests like coronene exhibit enhanced binding affinity when paired with electron-deficient arms **1**[211] compared to their neutral analogues **4**

and **5**.[199,212–214] The same types of interactions can facilitate self-association to form dimeric or polymeric complexes.[209] The structure of the arm can be further tuned to introduce additional properties. For example, incorporating chirality, as in **6** and **7**, induces a stereospecific twist in the complexed structures, and the resulting chiroptical signals in the absorption spectra are useful for circularly polarized light detection and chiroptical switching applications.[215,216] Increasing the number of arms can generate cooperative binding effects, as demonstrated by enhanced association in double-decker tweezers containing three arms.[217,218] These design strategies have proven valuable in the fabrication of supramolecular polymers, where the guest was modified to also contain two interacting arms similar to the host tweezers, affording association constants in the order of 10^6 M^{-1}.[192]

The structure of the tweezers' backbone can also be customized to achieve functional properties such as stimuli-responsiveness,[219] preorganization,[220] and supramolecular assembly.[191,221] In PAH-selective tweezers, the backbone generally consists of a combination of three benzene or pyridine rings to form terphenyl (**9**), diphenylpyridyl (**10**, **11**) or terpyridyl (**12**, **13**) frameworks. Molecular tweezers have also been synthetized using alternative backbones (**14, 15**), but their association constants to PAHs are generally lower, because the interplanar distance between the two arms deviates from the ~7 Å that is optimal for π-π stacking interactions.[195] Terpyridyl backbones like **12** and **13** can impart conformational switching through metal chelation, thereby functioning as an on/off switch for binding in those tweezers.[185,199,222,223] Alternative stimuli-responsive mechanisms have been reported (also by exploiting the structures of the arms and guest), including hydrogen bonding (with **11**, **16**),[192,224,225] pH changes (with **11**, **17**),[226,227] nucleophilic reactions (with **8**),[228] and redox processes (with **4**).[210]

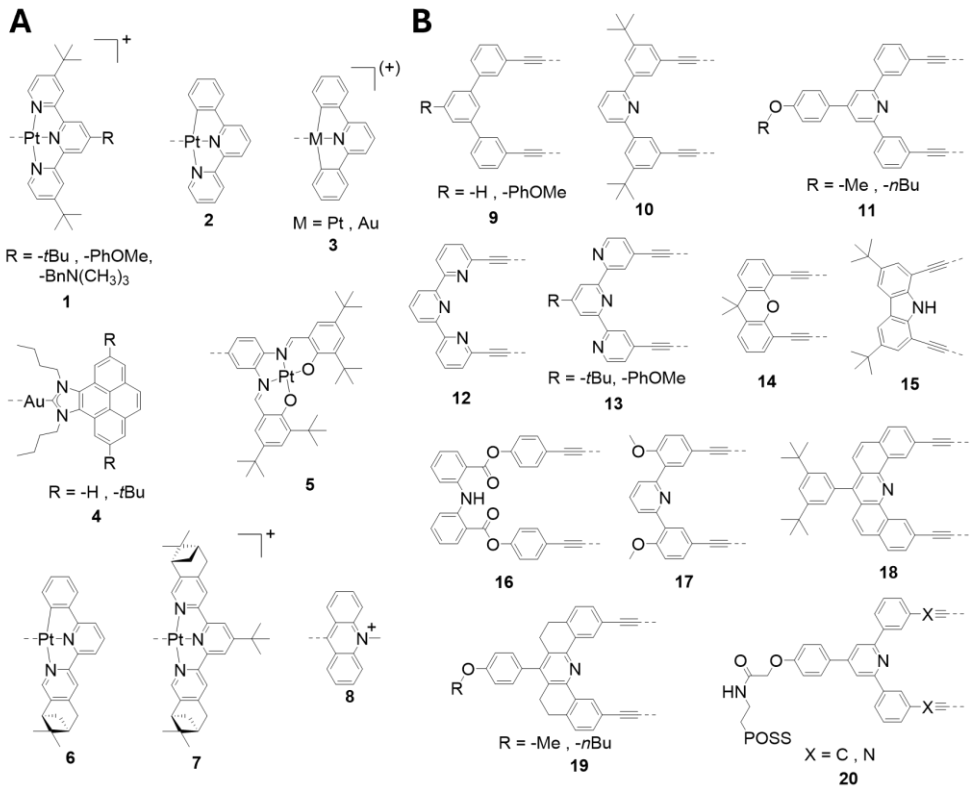

Figure 1.6 Structures of components in molecular tweezers developed for the binding of planar guests. (A) The arms of these molecular tweezers often consist of aromatic or organometallic moieties. (B) The backbone of these molecular tweezers generally consists of organic, aromatic compounds. Bn = benzyl, POSS = polyoctahedral silsesquioxane.

Table 1.1 The composition of several molecular tweezers and their reported dimerization constants ($K_{a,dim}$) and association constants towards polycyclic aromatic hydrocarbons ($K_{a,PAH}$) and organometallic complexes ($K_{a,OMC}$).

Arms	Backbone	$K_{a,PAH}$ (M^{-1})	$K_{a,OMC}$ (M^{-1}) [a]	$K_{a,dim}$ (M^{-1})	References
1 (R = *t*Bu)	**13** (R = *t*Bu)	n.d.	5.7×10^{4} [b]	Negligible [f]	Li et al.[184]
3 (M = Pt)	**20** (X = N)	n.d.	5.1×10^{3} [b]	50 [f]	Li et al.[184]
1 (R = OMe)	**11** (R = *n*Bu)	n.d.	9.5×10^{4} [f]	n.d.	Zhang et al.[189]
1 (R = *t*Bu)	**13** (R = PhOMe)	6.5×10^{4} [b,f]	$2.5 - 2.9 \times 10^{5}$ [h]	n.d.	Yuan et al.[185] Li et al.[223]
1 (R = *t*Bu)	**11** (R = *n*Bu)	2.3×10^{3} [c,f]	$1.3 - 3.1 \times 10^{4}$ [j]	Negligible [f]	Yuan et al.[85] Fu et al.[121] Gao et al.[226]

5	**13** (R = *t*Bu)	3.0×10^2 [d,f]	n.d.	n.d.	Benda et al.[199]
4 (R = *t*Bu)	**14**	$0.17 - 2.1 \times 10^3$ [c,f]	$<1.2 \times 10^2$ [f]	n.d.	Ibañez et al. [210]
4 (R = *t*Bu)	**15**	<10 [c,f] 1.4×10^2 [d,f]	n.d.	n.d.	Ibañez et al. [210,212]
1 (R = *t*Bu)	**10**	2.5×10^3 [c,f] 1.0×10^4 [d,f]	5.5×10^4 [k]	n.d.	Tanaka et al.[211,229]
4 (R = *t*Bu)	**18**	74 [c,f] 1.3×10^3 [d,f]	1.0×10^3 [f]	Stable	Ibañez et al.[212,214]
4 (R = *t*Bu)	**10**	1.9×10^3 [d,f]	9.5×10^2 [f]	n.d.	Ibañez [213]
4 (R = H)	**18**	n.d.	2.9×10^2 [f]	1.1×10^3 [f]	Ibañez et al. [214]
7	**11** (R = *n*Bu)	n.d.	7.0×10^4 [i] 1.2×10^4 [f]	5.3×10^2 [f] 1.3×10^3 [i]	Ren et al.[215]
6	**11** (R = *n*Bu)	n.d.	n.d.	Stable with Cu^+ [f]	Gao et al.[216]
5	**12**	Negligible [c,d]	n.d.	n.d.	Doisteau et al.[222]
1 (R = *t*Bu)	**11** (R = Me)	n.d.	4.7×10^4 [h]	Negligible [f]	Li et al.[223]
1 (R = *t*Bu)	**16**	n.d.	$1.2 - 1.3 \times 10^4$ [f]	n.d.	Lv et al.[224]
1 (R = $BnN(CH_3)_3$	**11** (R = *n*Bu)	n.d	$1.1 - 1.9 \times 10^4$ [j]	n.d.	Gao et al.[226]
9 (R = H)	**8**	10 [c,f]	n.d.	n.d.	Gosset et al.[228]
3 (M = Au)	**20** (X = C)	n.d.	$1.8 - 5.6 \times 10^5$ [f]	7.5×10^2 [f]	Zhong et al.[230]
3 (M = Au)	**11** (R = *n*Bu)	n.d.	5.2×10^5 [f]	n.d.	Zhong et al.[230]
1 (R = *t*Bu)	**9** (R = H)	50 [c,g] 6.4×10^2 [d,g]	n.d.	$<7.6 \times 10^2$ [f,g,i]	Nabeshima et al.[231]

n.d. not determined.

K_a values were measured at room temperature

[a] see reference for exact structure of the OMC as guest

[b] carbazole as guest

[c] pyrene as guest

[d] coronene as guest

[e] electron-deficient nitro-substituted PAHs as guests

[f] measured in chloroform

[g] measured in chloroform:acetonitrile 3:1

[h] measured in chloroform:acetonitrile 1:1

[i] measured in acetonitrile

[j] measured in DMSO

[k] measured in dichloromethane

Beyond stimuli-responsiveness, backbone design can also be exploited to introduce preorganization or self-assembly. While a flexible backbone offers substrate adaptability and stimuli-responsiveness, it also incurs entropic penalties associated with adopting the bound conformation.[220,232] In contrast, pre-organization minimizes these entropy costs and therefore enhances binding strengths. For instance, rigid dibenzoacridine backbones **18** and **19** possess increased binding affinities compared to their flexible diphenylpyridyl analogues **10** and **11**.[233] Finally, the backbone can be explored to alter material-oriented properties such as solubility or formation of supramolecular assemblies. The backbone provides a flexible platform compared to the arms for tuning solubility, as a large portion of the backbone is not positioned near the binding site. This adaptability allows the attachment of bulky substituents such as polyoctahedral silsesquioxane (POSS) units like in **20**, which can enhance solubility without compromising binding behaviour.[184] Moreover, the strategic design of POSS-functionalized tweezers has been demonstrated to promote supramolecular assembly into nanospheres.[230] In a different approach, attaching a pyrene binding moiety to the backbone facilitates head-to-tail association, resulting in linear supramolecular polymers.[186]

Among the wide variety of molecular tweezers described in the literature, one of them stands out as a suitable starting point for the purpose of graphene functionalization. Since graphene can be considered a large PAH, the choice of suitable tweezers was based on that perspective. Among the tweezers selective for large PAHs like pyrene and coronene (Figure 1.8),[192,199,211,212,231] the largest binding affinities towards PAHs was reported for the molecular tweezer consisting of a diphenyl pyridyl backbone **10** bearing two Pt(II)-terpyridine arms **1** developed by Tanaka et al.[229] This tweezer exhibited association constants in $CHCl_3$ of 10^3 M^{-1} and 10^4 M^{-1} for the binding of pyrene and coronene, respectively.[211] The tweezer's binding affinity was further evaluated across a series of PAHs ranging from two to seven rings, revealing a clear trend of increasing affinity with increasing size of the PAH, attributed to enhanced π–π interactions resulting from a larger π–surface area of the guest. Additionally, electron-donating substituents on the PAH were demonstrated to further increase the binding through enhanced charge-transfer interactions. In summary, their high binding affinity to large PAHs combined with extensive research into their intermolecular interactions, makes these tweezers a logical prototype for the binding of graphene.

Using molecular tweezers for graphene edge functionalization offers numerous advantages. First, the geometry of molecular tweezers makes them inherently selective for the edges of planar substrates. Second, since the functionalization with

molecular tweezers is non-covalent, this method is non-invasive and reversible. Third, molecular tweezers are highly versatile candidates for device functionalization. Attaching specific functional groups to the molecular tweezers allows graphene edges to be functionalized with those groups, adding specific properties. For example, a thiol linker can be used to anchor Au nanoparticles for enhanced visualization of graphene edges, a technique previously demonstrated with covalent functionalization methods.[174,175] Alternatively, functional groups can be added to slow down DNA translocation, as previously demonstrated by functionalizing nanopores with silanol or amine groups.[234] Indeed, this concept has also been demonstrated in amine-functionalized graphene fabricated through NH_3 plasma treatment.[156] By incorporating amine functional groups in the molecular tweezers and integrating them in graphene nanopore devices, similar effects could be achieved without the defect generation associated with plasma treatment. Fourth, the tweezers' binding affinity for graphene is dictated by non-covalent forces within the binding cavity. Therefore, the presence of various functional groups on the backbone is unlikely to affect the binding performance. This is different from for example diazonium chemistry, where different functional groups on aryldiazonium salts are known to alter their reactivity,[235–237] which limits the possible functional groups that can be added to graphene edges. Therefore, the possibilities of functional group integration using molecular tweezers are limited only by their synthesis. Finally, the tweezers' selectivity for graphene edges can be manipulated by incorporating specific groups (*e.g.* pyridines) near the binding cavity, which allows for specific non-covalent interactions (*e.g.* hydrogen bonding with amine-terminated graphene edges). As a result, the molecular tweezers are anticipated to be suitable for integration into all types of graphene nanopore devices, enabling tweezers-functionalized nanopore platforms for sequencing DNA, proteins, polysaccharides and other biopolymers.

One of the biggest challenges is the characterization of the molecular tweezers' interaction with graphene edges, which requires atomic resolution. Since tweezers-functionalized graphene has not been reported before, there is a need to understand the basics of these systems. While characterization using high-end instrumentation such as high-resolution TEM could provide visualization of the tweezers on the edges, the high-energy electron beam can cause damage to the graphene and organic molecules. Furthermore, this method is very demanding in operation and sample fabrication, which raises the risk of introducing preparation-induced artifacts. One way to circumvent these issues is to use soluble polycyclic aromatic hydrocarbons (PAHs) as target substrates, which serve as excellent graphene models.[9,238–242] The

solubility of PAHs in organic solvents allows the use of solution-based techniques such as NMR and UV-Vis spectroscopies for the characterization of their interactions with molecular tweezers.

1.6 Role of the solvent in host-guest chemistry

The solvent influences a range of physical and chemical properties and processes, such as color, stability, solubility, and reaction kinetics.[243] As a result, the solvent plays a crucial role in host-guest chemistry by affecting the binding affinity and selectivity.[244] However, in standard laboratory practice, the solvent is often only used to solubilize host or guest molecules, in which case its effect on host-guest complexation is disregarded. Although it is easy to use a solvent that has already been proven to be successful in similar studies, that does not mean that that solvent is necessarily optimal, for example, for maximizing binding affinity. This approach of imitating existing literature is understandable because selecting the optimal solvent is nontrivial, especially when the subtle interactions between a solute and the solvent are not completely understood and thus exceptionally challenging to predict. Therefore, even though the powerful influence of the solvent on chemical reactivity was discovered over a century ago,[245] many fields are still exploring the intimate relationships governed by these solvent effects.[246,247]

Primary concepts governing solvent effects on host-guest complexation are solvation and desolvation. Solvation describes the stabilization of a solute through non-covalent interactions with the solvent (Figure 1.7A, (i)→(ii)).[248] In thermodynamic terms, the Gibbs free energy of solvation of a mixture of a host and a guest (ΔG^0_S) can be quantified as the sum of the solvation Gibbs free energy of the host ($\Delta G^0_{S(H)}$) and of the guest ($\Delta G^0_{S(G)}$) (Figure 1.7B).[244] As a result, any solute is encapsulated by a solvation shell (also called hydration shell in water), which consists of solvent molecules that are ordered to a certain degree depending on the chemical properties of both the solvent and the solute. For example, in the case of water as the solvent, the solvation shell around a positively or negatively charged moiety is highly ordered due to water's strong directional dipole moment and hydrogen bonding properties, which can propagate several molecules into the bulk solution.[244,249] When the structure of the solute allows confinement of water molecules, for example, in hydrophobic cages or nanotubes, this hydrogen bonding network can even lead to the formation of "molecular ice", where confined water molecules behave as a solid rather than a liquid.[250,251] These solute-solvent interactions need to be displaced before solute-solute interactions can occur, which is called desolvation.

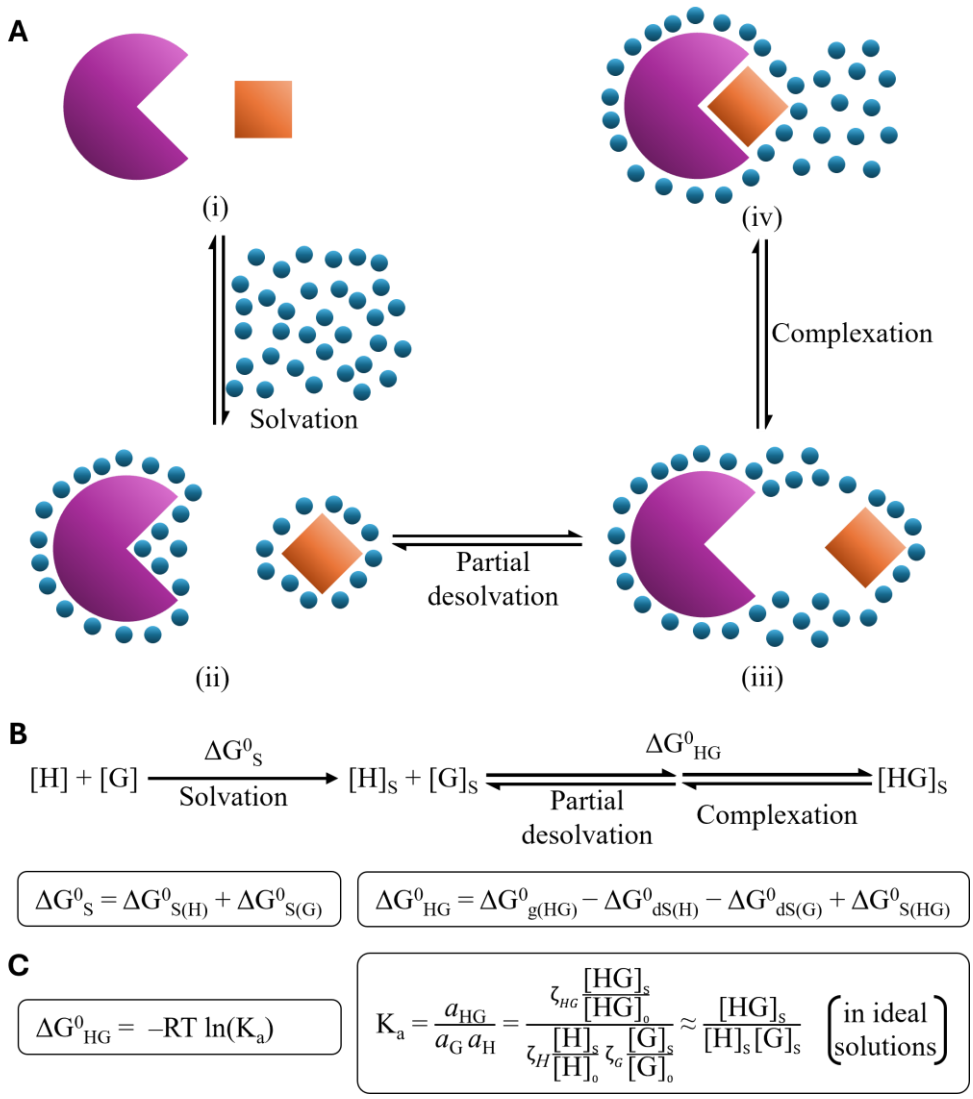

Figure 1.7 Solvation, partial desolvation, and complexation of a host and a guest molecule. (A) Illustration of the solvation (i)→(ii), partial desolvation (ii)→(iii), and complexation (iii)→(iv) of a host (purple partial circle) and a guest (orange square) in a solvent (blue spheres). (B) General equilibria and equations describing the Gibbs free energy of solvation (ΔG^0_S) and complexation (ΔG^0_{HG}) of a host (H) with its complementary guest molecule (G). (C) Relation between the Gibbs free energy of association in a solvent (ΔG_{HG}), association constant (K_a), and the activity of the host (a_H), guest (a_G), and host-guest complex (a_{HG}) in this solvent. The concentration values of the standard states for the host ($[H]_0$), guest ($[G]_0$), and host-guest complex ($[HG]_0$) are 1 M. In ideal solutions, the activity coefficient (ζ) of the solutes is 1, and the activity numerically equals the concentration (in M).[252]

Host-guest interactions generally require only partial desolvation, where solvent molecules in the binding pocket of the host and the respective interacting surface with the guest need to be displaced (Figure 1.7A, (ii)→(iii)). This displacement usually comes at a cost of a certain desolvation energy ($\Delta G^0_{dS(H)}$ and $\Delta G^0_{dS(G)}$ for the host and guest, respectively), which needs to be overcome by strong non-covalent interactions between the host and the guest ($\Delta G^0_{g(HG)}$, by definition in the gas phase) for effective complexation to occur (Figure 1.7A, (iii)→(iv)).[244] The stability of the supramolecular complex (ΔG^0_{HG}) can be described by the equilibrium between the components $\Delta G^0_{g(HG)}$, $\Delta G^0_{dS(H)}$, $\Delta G^0_{dS(G)}$, and the resulting solvation energy of the host-guest complex ($\Delta G^0_{S(HG)}$) (Figure 1.7B).[244] In practice, the binding affinity between a host and a guest can be quantified by the association constant (K_a), which relates the value of ΔG^0_{HG} to the concentrations of the host, guest, and complex in ideal solutions (Figure 1.7C).[244]

The effect of desolvation is particularly clear when studying hosts with initially empty cavities. For example, in the case of a cyclophane host and an imidazole guest, the association constants dramatically increased when the solvent was changed from a small molecule (K_a = 240 M^{-1} in dichloromethane) to large molecule (K_a = 1.28 × 10^5 M^{-1} in 1,1,2,2-tetrachloroethane).[253] The strong binding affinity in 1,1,2,2-tetrachloroethane was attributed to the exclusion of large solvent molecules from the host cavity, thereby eliminating solvent competition and the desolvation energy otherwise required for smaller solvent molecules prior to imidazole binding.[253]

A simple yet powerful parameter for analyzing solvent effects is solvent polarity. Solvent polarity determines its overall solvation capability as a result of all possible non-covalent interactions between the solvent and solute molecules.[243] Many linear free energy relationships (LFERs) have been demonstrated between the binding affinity of a host-guest complex and solvent polarity.[254] When plotting the binding affinity (quantified in ΔG^0_{HG}) vs. solvent polarity (quantified in *e.g.* $E_T(30)$), the binding affinity can either be correlated or inversely correlated with the solvent polarity. Typically, the sign of the correlation is determined by the specific host-guest system and is primarily driven by either solvophobic effects or electrostatic effects. In electrostatically driven complexation systems, such as bis(urea) host-cation binding, the binding affinity generally decreases with increasing solvent polarity.[255] The decrease in binding can be explained by screening of the electrostatic interactions between the host and guest in more polar solvents. In contrast, when considering systems based on hydrophobic or π-π stacking interactions, such as cyclophane cage-pyrene complexation, the binding affinity generally increases with increased solvent polarity, which can be attributed to solvophobic effects.[256–258] Still,

predicting the correlations is nontrivial, especially for complex systems in which both hydrophobic and hydrophilic moieties are present. For example, the binding of amines with zinc-porphyrin hosts, which is based on CH−π type interactions and steric repulsions, showed the lowest binding affinity in an intermediary solvent polarity rather than one of the outer extremes.[259] Similarly, the self-assembly of perylene bisimide (PBI) dye stacks, based on π-π stacking interactions, exhibited two linear correlations that separated a low-polarity domain from a high-polarity domain.[260] Additionally, LFERs based on solvent polarity often show exceptions or require categorization of different solvents (*e.g.* alcohols, amides, etc.).[260–262] Therefore, it is crucial to verify solvent effects in new systems empirically, especially since solvent polarity, which is generalized to encompass many different non-covalent interactions in solution, cannot describe specific interactions on the molecular level.[243]

Mixtures of two or more solvents are generally used to achieve intermediate solvent polarities, which is useful for characterizing complexation at solvent polarities that are otherwise unavailable with single-solvent systems.[255–259] However, the influence of solvent mixing on the resulting solvent polarity is nontrivial and depends heavily on the specific solvents. For example, mixing a hydrogen-accepting (DMF) and a hydrogen-donating ($CHCl_3$) solvent can result in a mixture with a solvent polarity higher than either of the individual solvents.[263] While this phenomenon does not necessarily mean that solvent polarity is a poor descriptor for binding affinity, it does emphasize the complexity of solvent polarity in solvent mixtures. Therefore, to fully understand the influence of solvent mixtures on a given host-guest system, comparing solvent polarity may be insufficient to give the complete model, especially since no solvent polarity scale is entirely universal.[264]

A practical consideration for choosing the right solvent for the characterization of a host-guest system is the solubility. Highly hydrophobic systems, such as Pt(II)-terpyridine tweezers and PAHs, naturally favor apolar, aprotic solvents such as chloroform.[192,199,211,212,231] Incorporation of solubilizing groups is often necessary to obtain sufficient solubility for spectroscopic characterization, especially for large PAHs which are notoriously poorly soluble.[242] Most Pt(II)-terpyridine molecular tweezers contain solubilizing groups on their backbone and/or their arms, such as *n*Bu, *t*Bu or POSS moieties (Figure 1.6 and Table 1.1). While solubilizing groups can be incorporated into the PAH,[265–268] such groups may sterically hinder their binding with molecular tweezers. Therefore, experimental, not *in silico*, studies on the binding of PAHs are limited to organic solvents.[9,241,269] Note that excessive

solubility would be detrimental to strong host-guest binding, because solvation competes directly with host-guest interactions (Figure 1.7).

1.7 Polycyclic aromatic hydrocarbons

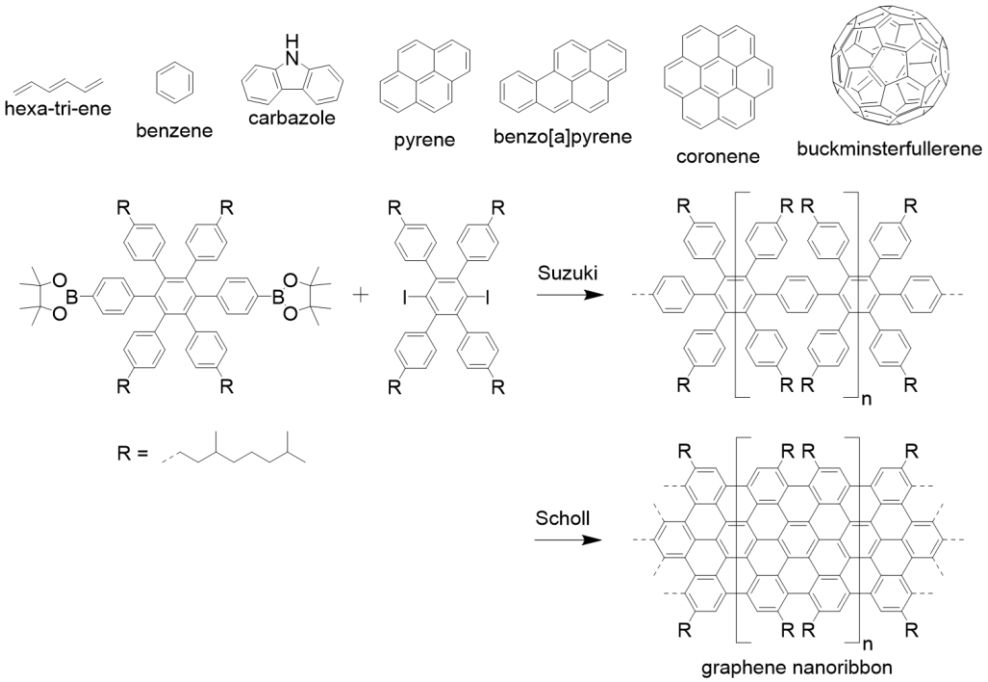

Figure 1.8 Chemical structures of exemplary PAHs and a bottom-up synthesis route of nanoribbons. Hexa-triene is the linear analogue of benzene, the simplest aromatic molecule. Carbazole, pyrene, and coronene are example targets for molecular tweezers in host-guest chemistry. Benzo[a]pyrene is notoriously carcinogenic and is widely studied in toxicology. Buckminsterfullerene is an example of exotic PAHs found in interstellar space. Graphene nanoribbons possess interesting properties in the field of materials science and can be synthetized from smaller PAH building blocks, for example *via* Suzuki and Scholl reactions.

Polycyclic aromatic hydrocarbons (PAHs) are a class of compounds consisting of at least two aromatic rings fused together. Though there may be some debate around the definition,[270] aromaticity in this thesis is defined as the concept of thermodynamic stabilization of the molecule as a result of cyclic electron delocalization.[271] The opposite of aromaticity is antiaromaticity, defined as a thermodynamic destabilization as a result of cyclic electron delocalization. Aromaticity or antiaromaticity can often be predicted simply using the chemical structure of the molecule. If the number of π-electrons in the molecule is n, aromatic molecules are usually obtained for $4n + 2$ electrons when the geometry of the PAHs

is linear monocyclic; this principle is known as Hückel's rule.[272–274] Notably, this rule does not always apply to polycyclic systems: for example pyrene and coronene have 16 and 24 π-electrons, respectively, but are still aromatic compounds. Second, the molecular topology should allow overlap of the π-orbitals. In other words, the molecule should be (mostly) planar so that the p_z-orbitals are parallel, which allows conjugation of p_z-electrons across the connecting σ-bonds. Finally, the structure should be cyclic so that the π-electrons are conjugated in a closed circuit. For example, benzene is a cyclic, aromatic analogue of hexa-triene (Figure 1.8). The stabilization resulting from cyclization is called the resonance energy. The stabilization resulting from aromaticity gives rise to many interesting properties, including a higher chemical stability,[275] specific reactivities (*e.g.*, aromatic electrophilic substitutions),[276] and magnetism.[277]

Research interest towards PAHs spans many fields, including toxicology, astronomy and materials science (Figure 1.8). PAHs are notorious for their carcinogenicity.[278–280] For example, benzo[a]pyrene contains reactive sites that allows metabolization into diol epoxides, which can bind to DNA and induce mutations.[281] In our everyday life, they are generated from incomplete combustion of organic matter, including burning of (fossil) fuels[282] and during food preparation.[283] The stability of aromatic compounds makes them resistant to degradation and more persistent in natural and synthetic environments.[279,280] PAHs are prevalent not only on Earth but also in space. Large PAHs, such as buckminsterfullerene (also known as buckyballs), are especially abundant in interstellar space, making them a central subject in astrochemistry.[284] Research in this field is critical for understanding processes such as star and planet formation, physical conditions in different galactic environments, and the origin of life.[285–288] In the fields of chemistry, PAHs are particularly interesting due to their unique optoelectronic properties.[289,290] Systematically altering the structure with dopants and substituents allows fine-tuning of molecular packing, absorption and fluorescence properties,[290–292] making them excellent building blocks in materials science such as organic field-effect transistors (OFETs)[293] and organic light-emitting diodes (OLEDs).[294] While research on the toxicological effects of PAHs are generally focused on PAHs smaller than six fused rings,[278–280] research on optoelectronic applications also extends to larger PAHs and graphene.[240,295,296]

Graphene is slightly different from conventional PAHs; it is not a molecule, but a 2D material characterized by the repeating structure of sp^2 carbon atoms arranged in a honeycomb pattern, resembling a PAH stretched out to infinity. Because graphene is an allotrope of carbon, it does not contain hydrogen by definition and is therefore classified as an inorganic material. Graphene is known for its exceptional mechanical

stability[133,134] and conductivity,[135,136] but its practical use is limited by the difficult fabrication of pristine, defect-free graphene. Graphene flakes and nanoribbons can be synthetized like any other PAH from smaller PAH building blocks through a combination of polymerization and ring closure reactions, including Ullman coupling, Diels-Alder, Suzuki, dehydrogenation and Scholl reactions.[297–299] While this method offers precise control over the chemistry of graphene structure and edges, the size of the graphene is limited by solubility issues. Other bottom-up synthesis techniques are based on carbon-carbon bond formation on a metal surface at high temperatures, such as Chemical Vapor Deposition (CVD), which uses small molecules like methane and ethene as carbon sources.[300,301] CVD can produce large quantities of graphene, especially when combined with instrumentation developed for roll-to-roll fabrication, however the quality of the graphene is generally compromised during the synthesis and transfer process.[302,303] Graphene produced through mechanical exfoliation from graphite possesses fewer defects and higher quality, however this fabrication method is incredibly difficult to scale up.[304,305] Due to the synthetic challenges, it is often easier to obtain graphene materials with pre-defined structures by post-synthetic functionalization.

1.8 Aim and outline of this thesis

Our goal is to develop a robust method to functionalize the graphene edges with molecular tweezers. To investigate whether molecular tweezers can serve as a suitable functionalization technique for graphene materials, several aspects need to be investigated. First, most molecular tweezers have been investigated in organic solvents, while DNA sequencing is generally performed in aqueous solvents. Therefore, it is important to understand the influence of the solvent on the binding. Second, understanding how the structure of the tweezers influences their binding properties to PAHs is imperative for rational optimization of the tweezers' design. Third, the relationship between the structure of graphene edges and its binding properties must be established to allow prediction and tuning of the functionalization based on edge chemistry. By using PAHs as graphene models, the binding can be characterized efficiently by using solution-based techniques. While many molecular tweezers have been developed to bind PAHs, few studies focus on how the solvent, host structure, and guest structure influence binding. The aim of this thesis is to fill in these knowledge gaps, as well as work towards improving the fabrication of graphene nanopores and other 2D materials.

Chapter 2 discusses how the binding interactions (quantified as the Gibbs free energy of association) of molecular tweezers can be influenced by their environment, which

is the solvent. We showed that in mixed-solvent systems, the Gibbs free energy of association (ΔG^0_a) could not be described by a single linear free-energy relationship (LFER) in contrast to single-solvent systems, which is often reported in literature. Instead, we observed that the value of ΔG^0_a could be described by two linear correlations as a function of solvent fraction, resulting in volcano plots. These results can be explained by the balance between two opposing solvent effects in mixed-solvent systems, namely solubilization vs. solvophobic effects, underscoring the complexity of host-guest-solvent interactions.

After understanding the solvent effects, the importance of the backbone structure of molecular tweezers was investigated in Chapter 3. Starting from molecular tweezers with a flexible backbone, we developed pre-organized molecular tweezers with a rigid backbone and a dodecyl chain to provide solubility in organic solvents. The influence of temperature on the binding is investigated, and the enthalpy, entropy and Gibbs free energy of association were determined. By changing the flexible backbone to a pre-organized one, the entropic penalty upon binding of the PAH was reduced. As a result, the new, pre-organized tweezers exhibited an increased binding affinity of 2 – 3 kJ mol^{-1}.

After developing molecular tweezers with higher affinity to PAHs in Chapter 3, the effect of the guest component on binding in the host-guest system was investigated in Chapter 4. The binding of seven planar PAHs with sizes varying from four to eight fused rings, six non-planar PAHs, and one nitrogen-containing PAH, to the molecular tweezers of Chapter 3, was investigated. We observed that the size of the PAH correlated with the binding affinity, while the shape determined its preferred orientation within the cavity of the molecular tweezers. Substituting carbons with nitrogen on the edge affected both the binding affinity and orientation. Moreover, the planarity of the PAH was demonstrated to be critical for binding to the tweezers.

Before applying molecular tweezers to graphene edges, we first investigated graphene nanopore fabrication in Chapter 5. We demonstrated the use of automated controlled breakdown (CBD) technique to provide a cheap, fast and accessible graphene nanopore fabrication method. Key fabrication parameters such as software controls, freestanding size of graphene, and solution conditions were investigated to understand and optimize the controlled breakdown process. Furthermore, the stability, multiporosity, and noise level of the fabricated nanopores were evaluated. These results underline the potential and limitations of CBD in graphene nanopore fabrication.

Chapter 6 explores the use of π-π stacking in the bottom-up synthesis of organized non-covalent 2D materials under ambient conditions as an alternative to conventional high-temperature methods like CVD or thermal annealing on metal surfaces. With the use of Langmuir-Blodgett technique, films with bimolecular thickness were fabricated on a water surface. These films were deposited on silicon, quartz and TEM-suitable substrates, which allowed detailed characterization of the film morphology, intermolecular interactions and freestanding ability in the film by atomic force microscopy (AFM), fluorescence spectroscopy and SEM, respectively. Chapter 6 demonstrates just one example of how far the field of π-π stacking in 2D materials can stretch beyond next-generation sequencing devices.

1.9 References

(1) Mayer, S. F.; Cao, C.; Dal Peraro, M. Biological Nanopores for Single-Molecule Sensing. *iScience* **2022**, *25* (4), 104145. https://doi.org/10.1016/j.isci.2022.104145.

(2) Wang, Y.; Wu, Z.; Meng, J. Understanding the Impact of Individual Nucleotide on Oxford Nanopore Current Signals With Interpretable Prediction Models. *Bioinforma. Biol. Insights* **2025**, *19*, 11779322251378620. https://doi.org/10.1177/11779322251378620.

(3) Schneider, G. F.; Dekker, C. DNA Sequencing with Nanopores. *Nat. Biotechnol.* **2012**, *30* (4), 326–328. https://doi.org/10.1038/nbt.2181.

(4) Qiu, H.; Zhou, W.; Guo, W. Nanopores in Graphene and Other 2D Materials: A Decade's Journey toward Sequencing. *ACS Nano* **2021**, *15* (12), 18848–18864. https://doi.org/10.1021/acsnano.1c07960.

(5) Bellunato, A.; Arjmandi Tash, H.; Cesa, Y.; et al. Chemistry at the Edge of Graphene. *ChemPhysChem* **2016**, *17* (6), 785–801. https://doi.org/10.1002/cphc.201500926.

(6) Lin, L.; Zhang, J.; Su, H.; et al. Towards Super-Clean Graphene. *Nat. Commun.* **2019**, *10* (1), 1912. https://doi.org/10.1038/s41467-019-09565-4.

(7) González, M. C. R.; Brown, A.; Eyley, S.; et al. Self-Limiting Covalent Modification of Carbon Surfaces: Diazonium Chemistry with a Twist. *Nanoscale* **2020**, *12* (36), 18782–18789. https://doi.org/10.1039/D0NR05244B.

(8) Zimmerman, S. C.; Zeng, Z.; Wu, W.; et al. Synthesis and Structure of Molecular Tweezers Containing Active Site Functionality. *J. Am. Chem. Soc.* **1991**, *113* (1), 183–196. https://doi.org/10.1021/ja00001a027.

(9) Mishra, P. C.; Yadav, A. Polycyclic Aromatic Hydrocarbons as Finite Size Models of Graphene and Graphene Nanoribbons: Enhanced Electron Density Edge Effect. *Chem. Phys.* **2012**, *402*, 56–68. https://doi.org/10.1016/j.chemphys.2012.04.005.

(10) Gautam, A. Applications of DNA Sequencing Technologies for Current Research. In *DNA and RNA Isolation Techniques for Non-Experts*; Gautam, A., Ed.; Springer International Publishing: Cham, **2022**; pp 179–195. https://doi.org/10.1007/978-3-030-94230-4_23.

(11) Miescher, F. Letter i; to Wilhelm His; Tübingen, February 26th, 1869. *Histochem Physiol Arb Friedrich Miescher-Aus Dem Wiss Briefwechsel Miescher* **1869**, *1*, 33–38.

(12) Dahm, R. Friedrich Miescher and the Discovery of DNA. *Dev. Biol.* **2005**, *278* (2), 274–288. https://doi.org/10.1016/j.ydbio.2004.11.028.

(13) Watson, J. D.; Crick, F. H. C. Molecular Structure of Nucleic Acids: A Structure for Deoxyribose Nucleic Acid. *Nature* **1953**, *171* (4356), 737–738. https://doi.org/10.1038/171737a0.

(14) Zallen, D. T. Despite Franklin's Work, Wilkins Earned His Nobel. *Nature* **2003**, *425* (6953), 15–15. https://doi.org/10.1038/425015b.

(15) Jou, W. M.; Haegeman, G.; Ysebaert, M.; et al. Nucleotide Sequence of the Gene Coding for the Bacteriophage MS2 Coat Protein. *Nature* **1972**, *237* (5350), 82–88. https://doi.org/10.1038/237082a0.

(16) Holley, R. W.; Madison, J. T.; Zamir, A. A New Method for Sequence Determination of Large Oligonucleotides. *Biochem. Biophys. Res. Commun.* **1964**, *17* (4), 389–394. https://doi.org/10.1016/0006-291X(64)90017-8.

(17) Holley, R. W.; Apgar, J.; Merrill, S. H.; et al. Nucleotide and Oligonucleotide Compositions of the Alanine-, Valine-, and Tyrosine-Acceptor "Soluble"

Ribonucleic Acids of Yeast. *J. Am. Chem. Soc.* **1961**, *83* (23), 4861–4862. https://doi.org/10.1021/ja01484a040.

(18) Sanger, F.; Air, G. M.; Barrell, B. G.; et al. Nucleotide Sequence of Bacteriophage φX174 DNA. *Nature* **1977**, *265* (5596), 687–695. https://doi.org/10.1038/265687a0.

(19) Sanger, F.; Nicklen, S.; Coulson, A. R. DNA Sequencing with Chain-Terminating Inhibitors. *Proc. Natl. Acad. Sci.* **1977**, *74* (12), 5463–5467. https://doi.org/10.1073/pnas.74.12.5463.

(20) Sanger, F.; Coulson, A. R. A Rapid Method for Determining Sequences in DNA by Primed Synthesis with DNA Polymerase. *J. Mol. Biol.* **1975**, *94* (3), 441–448. https://doi.org/10.1016/0022-2836(75)90213-2.

(21) Saiki, R. K.; Scharf, S.; Faloona, F.; et al. Enzymatic Amplification of β-Globin Genomic Sequences and Restriction Site Analysis for Diagnosis of Sickle Cell Anemia. *Science* **1985**, *230* (4732), 1350–1354. https://doi.org/10.1126/science.2999980.

(22) Saiki, R. K.; Gelfand, D. H.; Stoffel, S.; et al. Primer-Directed Enzymatic Amplification of DNA with a Thermostable DNA Polymerase. *Science* **1988**, *239* (4839), 487–491. https://doi.org/10.1126/science.2448875.

(23) Staden, R. A Strategy of DNA Sequencing Employing Computer Programs. *Nucleic Acids Res.* **1979**, *6* (7), 2601–2610. https://doi.org/10.1093/nar/6.7.2601.

(24) Anderson, S. Shotgun DNA Sequencing Using Cloned DNase I-Generated Fragments. *Nucleic Acids Res.* **1981**, *9* (13), 3015–3027. https://doi.org/10.1093/nar/9.13.3015.

(25) Hunkapiller, T.; Kaiser, R. J.; Koop, B. F.; et al. Large-Scale and Automated DNA Sequence Determination. *Science* **1991**, *254* (5028), 59–67. https://doi.org/10.1126/science.1925562.

(26) International Human Genome Sequencing Consortium. Finishing the Euchromatic Sequence of the Human Genome. *Nature* **2004**, *431* (7011), 931–945. https://doi.org/10.1038/nature03001.

(27) Margulies, M.; Egholm, M.; Altman, W. E.; et al. Genome Sequencing in Microfabricated High-Density Picolitre Reactors. *Nature* **2005**, *437* (7057), 376–380. https://doi.org/10.1038/nature03959.

(28) Valouev, A.; Ichikawa, J.; Tonthat, T.; et al. A High-Resolution, Nucleosome Position Map of *C. Elegans* Reveals a Lack of Universal Sequence-Dictated Positioning. *Genome Res.* **2008**, *18* (7), 1051–1063. https://doi.org/10.1101/gr.076463.108.

(29) Rusk, N. Torrents of Sequence. *Nat. Methods* **2011**, *8* (1), 44–44. https://doi.org/10.1038/nmeth.f.330.

(30) Bentley, D. R.; Balasubramanian, S.; Swerdlow, H. P.; et al. Accurate Whole Human Genome Sequencing Using Reversible Terminator Chemistry. *Nature* **2008**, *456* (7218), 53–59. https://doi.org/10.1038/nature07517.

(31) Lerminiaux, N.; Fakharuddin, K.; Mulvey, M. R.; et al. Do We Still Need Illumina Sequencing Data? Evaluating Oxford Nanopore Technologies R10.4.1 Flow Cells and the Rapid V14 Library Prep Kit for Gram Negative Bacteria Whole Genome Assemblies. *Can. J. Microbiol.* **2024**, *70* (5), 178–189. https://doi.org/10.1139/cjm-2023-0175.

(32) Turcatti, G.; Romieu, A.; Fedurco, M.; et al. A New Class of Cleavable Fluorescent Nucleotides: Synthesis and Optimization as Reversible Terminators for DNA

Sequencing by Synthesis. *Nucleic Acids Res.* **2008**, *36* (4), e25. https://doi.org/10.1093/nar/gkn021.

(33) Fedurco, M.; Romieu, A.; Williams, S.; et al. BTA, a Novel Reagent for DNA Attachment on Glass and Efficient Generation of Solid-Phase Amplified DNA Colonies. *Nucleic Acids Res.* **2006**, *34* (3), e22. https://doi.org/10.1093/nar/gnj023.

(34) Koren, S.; Phillippy, A. M. One Chromosome, One Contig: Complete Microbial Genomes from Long-Read Sequencing and Assembly. *Curr. Opin. Microbiol.* **2015**, *23*, 110–120. https://doi.org/10.1016/j.mib.2014.11.014.

(35) Chaisson, M. J. P.; Huddleston, J.; Dennis, M. Y.; et al. Resolving the Complexity of the Human Genome Using Single-Molecule Sequencing. *Nature* **2015**, *517* (7536), 608–611. https://doi.org/10.1038/nature13907.

(36) Jain, M.; Olsen, H. E.; Paten, B.; et al. The Oxford Nanopore MinION: Delivery of Nanopore Sequencing to the Genomics Community. *Genome Biol.* **2016**, *17* (1), 239. https://doi.org/10.1186/s13059-016-1103-0.

(37) Haque, F.; Li, J.; Wu, H.-C.; et al. Solid-State and Biological Nanopore for Real-Time Sensing of Single Chemical and Sequencing of DNA. *Nano Today* **2013**, *8* (1), 56–74. https://doi.org/10.1016/j.nantod.2012.12.008.

(38) Hogg, W. R.; Coulter, W. H. Apparatus and Method for Measuring a Dividing Particle Size of a Particulate System. US3557352A, January 19, **1971**. https://patents.google.com/patent/US3557352A/en.

(39) Mason, C. E.; Elemento, O. Faster Sequencers, Larger Datasets, New Challenges. *Genome Biol.* **2012**, *13* (3), 314. https://doi.org/10.1186/gb-2012-13-3-314.

(40) Meslier, V.; Quinquis, B.; Da Silva, K.; et al. Benchmarking Second and Third-Generation Sequencing Platforms for Microbial Metagenomics. *Sci. Data* **2022**, *9* (1), 694. https://doi.org/10.1038/s41597-022-01762-z.

(41) Wang, Y.; Zhao, Y.; Bollas, A.; et al. Nanopore Sequencing Technology, Bioinformatics and Applications. *Nat. Biotechnol.* **2021**, *39* (11), 1348–1365. https://doi.org/10.1038/s41587-021-01108-x.

(42) Menestrina, G. Ionic Channels Formed by *Staphylococcus Aureus* Alpha-Toxin: Voltage-Dependent Inhibition by Divalent and Trivalent Cations. *J. Membr. Biol.* **1986**, *90* (2), 177–190. https://doi.org/10.1007/BF01869935.

(43) Song, L.; Hobaugh, M. R.; Shustak, C.; et al. Structure of Staphylococcal α-Hemolysin, a Heptameric Transmembrane Pore. *Science* **1996**, *274* (5294), 1859–1865. https://doi.org/10.1126/science.274.5294.1859.

(44) Niederweis, M.; Ehrt, S.; Heinz, C.; et al. Cloning of the *mspA* Gene Encoding a Porin from *Mycobacterium Smegmatis*. *Mol. Microbiol.* **1999**, *33* (5), 933–945. https://doi.org/10.1046/j.1365-2958.1999.01472.x.

(45) Faller, M.; Niederweis, M.; Schulz, G. E. The Structure of a Mycobacterial Outer-Membrane Channel. *Science* **2004**, *303* (5661), 1189–1192. https://doi.org/10.1126/science.1094114.

(46) Kasianowicz, J. J.; Brandin, E.; Branton, D.; et al. Characterization of Individual Polynucleotide Molecules Using a Membrane Channel. *Proc. Natl. Acad. Sci.* **1996**, *93* (24), 13770–13773. https://doi.org/10.1073/pnas.93.24.13770.

(47) Butler, T. Z.; Pavlenok, M.; Derrington, I. M.; et al. Single-Molecule DNA Detection with an Engineered MspA Protein Nanopore. *Proc. Natl. Acad. Sci.* **2008**, *105* (52), 20647–20652. https://doi.org/10.1073/pnas.0807514106.

(48) Derrington, I. M.; Butler, T. Z.; Collins, M. D.; et al. Nanopore DNA Sequencing with MspA. *Proc. Natl. Acad. Sci.* **2010**, *107* (37), 16060–16065. https://doi.org/10.1073/pnas.1001831107.
(49) Meller, A. Dynamics of Polynucleotide Transport through Nanometre-Scale Pores. *J. Phys. Condens. Matter* **2003**, *15* (17), R581. https://doi.org/10.1088/0953-8984/15/17/202.
(50) Branton, D.; Deamer, D. W.; Marziali, A.; et al. The Potential and Challenges of Nanopore Sequencing. *Nat. Biotechnol.* **2008**, *26* (10), 1146–1153. https://doi.org/10.1038/nbt.1495.
(51) Deamer, D. W.; Branton, D. Characterization of Nucleic Acids by Nanopore Analysis. *Acc. Chem. Res.* **2002**, *35* (10), 817–825. https://doi.org/10.1021/ar000138m.
(52) Lieberman, K. R.; Cherf, G. M.; Doody, M. J.; et al. Processive Replication of Single DNA Molecules in a Nanopore Catalyzed by Phi29 DNA Polymerase. *J. Am. Chem. Soc.* **2010**, *132* (50), 17961–17972. https://doi.org/10.1021/ja1087612.
(53) Cherf, G. M.; Lieberman, K. R.; Rashid, H.; et al. Automated Forward and Reverse Ratcheting of DNA in a Nanopore at 5-Å Precision. *Nat. Biotechnol.* **2012**, *30* (4), 344–348. https://doi.org/10.1038/nbt.2147.
(54) Hornblower, B.; Coombs, A.; Whitaker, R. D.; et al. Single-Molecule Analysis of DNA-Protein Complexes Using Nanopores. *Nat. Methods* **2007**, *4* (4), 315–317. https://doi.org/10.1038/nmeth1021.
(55) Benner, S.; Chen, R. J. A.; Wilson, N. A.; et al. Sequence-Specific Detection of Individual DNA Polymerase Complexes in Real Time Using a Nanopore. *Nat. Nanotechnol.* **2007**, *2* (11), 718–724. https://doi.org/10.1038/nnano.2007.344.
(56) Cockroft, S. L.; Chu, J.; Amorin, M.; et al. A Single-Molecule Nanopore Device Detects DNA Polymerase Activity with Single-Nucleotide Resolution. *J. Am. Chem. Soc.* **2008**, *130* (3), 818–820. https://doi.org/10.1021/ja077082c.
(57) Manrao, E. A.; Derrington, I. M.; Laszlo, A. H.; et al. Reading DNA at Single-Nucleotide Resolution with a Mutant MspA Nanopore and Phi29 DNA Polymerase. *Nat. Biotechnol.* **2012**, *30* (4), 349–353. https://doi.org/10.1038/nbt.2171.
(58) Payne, A.; Holmes, N.; Rakyan, V.; et al. BulkVis: A Graphical Viewer for Oxford Nanopore Bulk FAST5 Files. *Bioinformatics* **2019**, *35* (13), 2193–2198. https://doi.org/10.1093/bioinformatics/bty841.
(59) *Nanopore store: Ultra-Long DNA Sequencing Kit V14*. https://store.nanoporetech.com/us/ultra-long-dna-sequencing-kit-v14.html (accessed 2025-09-18).
(60) Kolmogorov, M.; Billingsley, K. J.; Mastoras, M.; et al. Scalable Nanopore Sequencing of Human Genomes Provides a Comprehensive View of Haplotype-Resolved Variation and Methylation. *Nat. Methods* **2023**, *20* (10), 1483–1492. https://doi.org/10.1038/s41592-023-01993-x.
(61) *Nanopore sequencing accuracy*. Oxford Nanopore Technologies. https://nanoporetech.com/platform/accuracy (accessed 2025-09-18).
(62) Glencross, F.; Khan, D. A. *BioRender*. Nanopore Sequencing. https://app.biorender.com/biorender-templates/t-5f8717bcfb2c3900a82de0ae (accessed 2025-09-30).
(63) Schneider, G. F.; Kowalczyk, S. W.; Calado, V. E.; et al. DNA Translocation through Graphene Nanopores. *Nano Lett.* **2010**, *10* (8), 3163–3167. https://doi.org/10.1021/nl102069z.

(64) Merchant, C. A.; Healy, K.; Wanunu, M.; et al. DNA Translocation through Graphene Nanopores. *Nano Lett.* **2010**, *10* (8), 2915–2921. https://doi.org/10.1021/nl101046t.
(65) Garaj, S.; Hubbard, W.; Reina, A.; et al. Graphene as a Subnanometre Trans-Electrode Membrane. *Nature* **2010**, *467* (7312), 190–193. https://doi.org/10.1038/nature09379.
(66) Mohammadi, M. M.; Bavi, O. DNA Sequencing: An Overview of Solid-State and Biological Nanopore-Based Methods. *Biophys. Rev.* **2022**, *14* (1), 99–110. https://doi.org/10.1007/s12551-021-00857-y.
(67) Ying, Y.-L.; Hu, Z.-L.; Zhang, S.; et al. Nanopore-Based Technologies beyond DNA Sequencing. *Nat. Nanotechnol.* **2022**, *17* (11), 1136–1146. https://doi.org/10.1038/s41565-022-01193-2.
(68) He, Y.; Tsutsui, M.; Zhou, Y.; et al. Solid-State Nanopore Systems: From Materials to Applications. *NPG Asia Mater.* **2021**, *13* (1), 48. https://doi.org/10.1038/s41427-021-00313-z.
(69) Venta, K.; Shemer, G.; Puster, M.; et al. Differentiation of Short, Single-Stranded DNA Homopolymers in Solid-State Nanopores. *ACS Nano* **2013**, *7* (5), 4629–4636. https://doi.org/10.1021/nn4014388.
(70) Storm, A. J.; Chen, J. H.; Zandbergen, H. W.; et al. Translocation of Double-Strand DNA through a Silicon Oxide Nanopore. *Phys. Rev. E* **2005**, *71* (5), 051903. https://doi.org/10.1103/PhysRevE.71.051903.
(71) Venkatesan, B. M.; Dorvel, B.; Yemenicioglu, S.; et al. Highly Sensitive, Mechanically Stable Nanopore Sensors for DNA Analysis. *Adv. Mater.* **2009**, *21* (27), 2771–2776. https://doi.org/10.1002/adma.200803786.
(72) Larkin, J.; Henley, R.; Bell, D. C.; et al. Slow DNA Transport through Nanopores in Hafnium Oxide Membranes. *ACS Nano* **2013**, *7* (11), 10121–10128. https://doi.org/10.1021/nn404326f.
(73) Park, K.-B.; Kim, H.-J.; Kang, Y.-H.; et al. Highly Reliable and Low-Noise Solid-State Nanopores with an Atomic Layer Deposited ZnO Membrane on a Quartz Substrate. *Nanoscale* **2017**, *9* (47), 18772–18780. https://doi.org/10.1039/C7NR05755E.
(74) Nouri, R.; Tang, Z.; Guan, W. Quantitative Analysis of Factors Affecting the Event Rate in Glass Nanopore Sensors. *ACS Sens.* **2019**, *4* (11), 3007–3013. https://doi.org/10.1021/acssensors.9b01540.
(75) Yusko, E. C.; Johnson, J. M.; Majd, S.; et al. Controlling Protein Translocation through Nanopores with Bio-Inspired Fluid Walls. *Nat. Nanotechnol.* **2011**, *6* (4), 253–260. https://doi.org/10.1038/nnano.2011.12.
(76) Talaga, D. S.; Li, J. Single-Molecule Protein Unfolding in Solid State Nanopores. *J. Am. Chem. Soc.* **2009**, *131* (26), 9287–9297. https://doi.org/10.1021/ja901088b.
(77) Sha, J.; Si, W.; Xu, B.; et al. Identification of Spherical and Nonspherical Proteins by a Solid-State Nanopore. *Anal. Chem.* **2018**, *90* (23), 13826–13831. https://doi.org/10.1021/acs.analchem.8b04136.
(78) Yusko, E. C.; Bruhn, B. R.; Eggenberger, O. M.; et al. Real-Time Shape Approximation and Fingerprinting of Single Proteins Using a Nanopore. *Nat. Nanotechnol.* **2017**, *12* (4), 360–367. https://doi.org/10.1038/nnano.2016.267.
(79) Ervin, E. N.; Barrall, G. A.; Pal, P.; et al. Creating a Single Sensing Zone Within an Alpha-Hemolysin Pore *via* Site-Directed Mutagenesis. *BioNanoScience* **2014**, *4* (1), 78–84. https://doi.org/10.1007/s12668-013-0119-0.

(80) Niedringhaus, T. P.; Milanova, D.; Kerby, M. B.; et al. Landscape of Next-Generation Sequencing Technologies. *Anal. Chem.* **2011**, *83* (12), 4327–4341. https://doi.org/10.1021/ac2010857.

(81) Mandelkern, M.; Elias, J. G.; Eden, D.; et al. The Dimensions of DNA in Solution. *J. Mol. Biol.* **1981**, *152* (1), 153–161. https://doi.org/10.1016/0022-2836(81)90099-1.

(82) Ramazi, S.; Zahiri, J. Post-Translational Modifications in Proteins: Resources, Tools and Prediction Methods. *Database* **2021**, *2021*, baab012. https://doi.org/10.1093/database/baab012.

(83) Novoselov, K. S.; Geim, A. K.; Morozov, S. V.; et al. Electric Field Effect in Atomically Thin Carbon Films. *Science* **2004**, *306* (5696), 666–669. https://doi.org/10.1126/science.1102896.

(84) Zhou, Z.; Hu, Y.; Wang, H.; et al. DNA Translocation through Hydrophilic Nanopore in Hexagonal Boron Nitride. *Sci. Rep.* **2013**, *3* (1), 3287. https://doi.org/10.1038/srep03287.

(85) Liu, K.; Feng, J.; Kis, A.; et al. Atomically Thin Molybdenum Disulfide Nanopores with High Sensitivity for DNA Translocation. *ACS Nano* **2014**, *8* (3), 2504–2511. https://doi.org/10.1021/nn406102h.

(86) Mojtabavi, M.; VahidMohammadi, A.; Liang, W.; et al. Single-Molecule Sensing Using Nanopores in Two-Dimensional Transition Metal Carbide (MXene) Membranes. *ACS Nano* **2019**, *13* (3), 3042–3053. https://doi.org/10.1021/acsnano.8b08017.

(87) Heerema, S. J.; Vicarelli, L.; Pud, S.; et al. Probing DNA Translocations with Inplane Current Signals in a Graphene Nanoribbon with a Nanopore. *ACS Nano* **2018**, *12* (3), 2623–2633. https://doi.org/10.1021/acsnano.7b08635.

(88) Niedzwiecki, D. J.; Grazul, J.; Movileanu, L. Single-Molecule Observation of Protein Adsorption onto an Inorganic Surface. *J. Am. Chem. Soc.* **2010**, *132* (31), 10816–10822. https://doi.org/10.1021/ja1026858.

(89) Freedman, K. J.; Haq, S. R.; Fletcher, M. R.; et al. Nonequilibrium Capture Rates Induce Protein Accumulation and Enhanced Adsorption to Solid-State Nanopores. *ACS Nano* **2014**, *8* (12), 12238–12249. https://doi.org/10.1021/nn5062645.

(90) Li, S.; Zeng, S.; Wen, C.; et al. Docking and Activity of DNA Polymerase on Solid-State Nanopores. *ACS Sens.* **2022**, *7* (5), 1476–1483. https://doi.org/10.1021/acssensors.2c00216.

(91) Zhou, Y.; Long, X.; Zhang, Y.; et al. Advances and Challenges in Solid-State Nanopores for DNA Sequencing. *Langmuir* **2025**, *41* (9), 5736–5761. https://doi.org/10.1021/acs.langmuir.4c04961.

(92) Wanunu, M.; Sutin, J.; McNally, B.; et al. DNA Translocation Governed by Interactions with Solid-State Nanopores. *Biophys. J.* **2008**, *95* (10), 4716–4725. https://doi.org/10.1529/biophysj.108.140475.

(93) Akahori, R.; Haga, T.; Hatano, T.; et al. Slowing Single-Stranded DNA Translocation through a Solid-State Nanopore by Decreasing the Nanopore Diameter. *Nanotechnology* **2014**, *25* (27), 275501. https://doi.org/10.1088/0957-4484/25/27/275501.

(94) Liang, L.; Cui, P.; Wang, Q.; et al. Theoretical Study on Key Factors in DNA Sequencing with Graphene Nanopores. *RSC Adv.* **2013**, *3* (7), 2445–2453. https://doi.org/10.1039/C2RA22109H.

(95) Verschueren, D. V.; Jonsson, M. P.; Dekker, C. Temperature Dependence of DNA Translocations through Solid-State Nanopores. *Nanotechnology* **2015**, *26* (23), 234004. https://doi.org/10.1088/0957-4484/26/23/234004.

(96) Feng, J.; Liu, K.; Bulushev, R. D.; et al. Identification of Single Nucleotides in MoS2 Nanopores. *Nat. Nanotechnol.* **2015**, *10* (12), 1070–1076. https://doi.org/10.1038/nnano.2015.219.

(97) Plesa, C.; Loo, N. van; Dekker, C. DNA Nanopore Translocation in Glutamate Solutions. *Nanoscale* **2015**, *7* (32), 13605–13609. https://doi.org/10.1039/C5NR02793D.

(98) Soni, N.; Chandra Verma, N.; Talor, N.; et al. Over 30-Fold Enhancement in DNA Translocation Dynamics through Nanoscale Pores Coated with an Anionic Surfactant. *Nano Lett.* **2023**, *23* (10), 4609–4616. https://doi.org/10.1021/acs.nanolett.3c01096.

(99) He, Y.; Tsutsui, M.; Fan, C.; et al. Controlling DNA Translocation through Gate Modulation of Nanopore Wall Surface Charges. *ACS Nano* **2011**, *5* (7), 5509–5518. https://doi.org/10.1021/nn201883b.

(100) Goto, Y.; Matsui, K.; Yanagi, I.; et al. Silicon Nitride Nanopore Created by Dielectric Breakdown with a Divalent Cation: Deceleration of Translocation Speed and Identification of Single Nucleotides. *Nanoscale* **2019**, *11* (30), 14426–14433. https://doi.org/10.1039/C9NR03563J.

(101) Yanagi, I.; Akahori, R.; Takeda, K. Dwell Time Prolongation and Identification of Single Nucleotides Passing through a Solid-State Nanopore by Using Ammonium Sulfate Aqueous Solution. *ACS Omega* **2023**, *8* (23), 21285–21292. https://doi.org/10.1021/acsomega.3c02703.

(102) Smeets, R. M. M.; Keyser, U. F.; Krapf, D.; et al. Salt Dependence of Ion Transport and DNA Translocation through Solid-State Nanopores. *Nano Lett.* **2006**, *6* (1), 89–95. https://doi.org/10.1021/nl052107w.

(103) Luan, B.; Aksimentiev, A. Electric and Electrophoretic Inversion of the DNA Charge in Multivalent Electrolytes. *Soft Matter* **2010**, *6* (2), 243–246. https://doi.org/10.1039/B917973A.

(104) Kowalczyk, S. W.; Wells, D. B.; Aksimentiev, A.; et al. Slowing down DNA Translocation through a Nanopore in Lithium Chloride. *Nano Lett.* **2012**, *12* (2), 1038–1044. https://doi.org/10.1021/nl204273h.

(105) Chinappi, M.; Yamaji, M.; Kawano, R.; et al. Analytical Model for Particle Capture in Nanopores Elucidates Competition among Electrophoresis, Electroosmosis, and Dielectrophoresis. *ACS Nano* **2020**, *14* (11), 15816–15828. https://doi.org/10.1021/acsnano.0c06981.

(106) Pud, S.; Chao, S.-H.; Belkin, M.; et al. Mechanical Trapping of DNA in a Double-Nanopore System. *Nano Lett.* **2016**, *16* (12), 8021–8028. https://doi.org/10.1021/acs.nanolett.6b04642.

(107) Keyser, U. F.; Koeleman, B. N.; van Dorp, S.; et al. Direct Force Measurements on DNA in a Solid-State Nanopore. *Nat. Phys.* **2006**, *2* (7), 473–477. https://doi.org/10.1038/nphys344.

(108) Peng, H.; Ling, X. S. Reverse DNA Translocation through a Solid-State Nanopore by Magnetic Tweezers. *Nanotechnology* **2009**, *20* (18), 185101. https://doi.org/10.1088/0957-4484/20/18/185101.

(109) Kim, J.-D.; Lee, Y.-G. Trapping of a Single DNA Molecule Using Nanoplasmonic Structures for Biosensor Applications. *Biomed. Opt. Express* **2014**, *5* (8), 2471–2480. https://doi.org/10.1364/BOE.5.002471.
(110) Belkin, M.; Chao, S.-H.; Jonsson, M. P.; et al. Plasmonic Nanopores for Trapping, Controlling Displacement, and Sequencing of DNA. *ACS Nano* **2015**, *9* (11), 10598–10611. https://doi.org/10.1021/acsnano.5b04173.
(111) Si, W.; Yang, H.; Wu, G.; et al. Manipulation of DNA Transport through Solid-State Nanopores by Atomic Force Microscopy. *Mater. Res. Express* **2020**, *7* (9), 095404. https://doi.org/10.1088/2053-1591/abb856.
(112) Hyun, C.; Kaur, H.; Rollings, R.; et al. Threading Immobilized DNA Molecules through a Solid-State Nanopore at >100 μs per Base Rate. *ACS Nano* **2013**, *7* (7), 5892–5900. https://doi.org/10.1021/nn4012434.
(113) Akahori, R.; Yanagi, I.; Goto, Y.; et al. Discrimination of Three Types of Homopolymers in Single-Stranded DNA with Solid-State Nanopores through External Control of the DNA Motion. *Sci. Rep.* **2017**, *7* (1), 9073. https://doi.org/10.1038/s41598-017-08290-6.
(114) Yuan, Z.; Liu, Y.; Dai, M.; et al. Controlling DNA Translocation Through Solid-State Nanopores. *Nanoscale Res. Lett.* **2020**, *15* (1), 80. https://doi.org/10.1186/s11671-020-03308-x.
(115) Ashkin, A.; Dziedzic, J. M.; Bjorkholm, J. E.; et al. Observation of a Single-Beam Gradient Force Optical Trap for Dielectric Particles. *Opt. Lett.* **1986**, *11* (5), 288–290. https://doi.org/10.1364/OL.11.000288.
(116) Li, Y.; Nicoli, F.; Chen, C.; et al. Photoresistance Switching of Plasmonic Nanopores. *Nano Lett.* **2015**, *15* (1), 776–782. https://doi.org/10.1021/nl504516d.
(117) Zhang, Y.; Min, C.; Dou, X.; et al. Plasmonic Tweezers: For Nanoscale Optical Trapping and Beyond. *Light Sci. Appl.* **2021**, *10* (1), 59. https://doi.org/10.1038/s41377-021-00474-0.
(118) Keyser, U. F.; Krapf, D.; Koeleman, B. N.; et al. Nanopore Tomography of a Laser Focus. *Nano Lett.* **2005**, *5* (11), 2253–2256. https://doi.org/10.1021/nl051597p.
(119) Nelson, E. M.; Li, H.; Timp, G. Direct, Concurrent Measurements of the Forces and Currents Affecting DNA in a Nanopore with Comparable Topography. *ACS Nano* **2014**, *8* (6), 5484–5493. https://doi.org/10.1021/nn405331t.
(120) Li, W.; Zhou, J.; Maccaferri, N.; et al. Enhanced Optical Spectroscopy for Multiplexed DNA and Protein-Sequencing with Plasmonic Nanopores: Challenges and Prospects. *Anal. Chem.* **2022**, *94* (2), 503–514. https://doi.org/10.1021/acs.analchem.1c04459.
(121) Assad, O. N.; Gilboa, T.; Spitzberg, J.; et al. Light-Enhancing Plasmonic-Nanopore Biosensor for Superior Single-Molecule Detection. *Adv. Mater.* **2017**, *29* (9), 1605442. https://doi.org/10.1002/adma.201605442.
(122) Xie, P.; Xiong, Q.; Fang, Y.; et al. Local Electrical Potential Detection of DNA by Nanowire–Nanopore Sensors. *Nat. Nanotechnol.* **2012**, *7* (2), 119–125. https://doi.org/10.1038/nnano.2011.217.
(123) Graf, M.; Lihter, M.; Altus, D.; et al. Transverse Detection of DNA Using a MoS2 Nanopore. *Nano Lett.* **2019**, *19* (12), 9075–9083. https://doi.org/10.1021/acs.nanolett.9b04180.
(124) Soni, G. V.; Meller, A. Progress toward Ultrafast DNA Sequencing Using Solid-State Nanopores. *Clin. Chem.* **2007**, *53* (11), 1996–2001. https://doi.org/10.1373/clinchem.2007.091231.

(125) McNally, B.; Singer, A.; Yu, Z.; et al. Optical Recognition of Converted DNA Nucleotides for Single-Molecule DNA Sequencing Using Nanopore Arrays. *Nano Lett.* **2010**, *10* (6), 2237–2244. https://doi.org/10.1021/nl1012147.
(126) Lagerqvist, J.; Zwolak, M.; Di Ventra, M. Fast DNA Sequencing *via* Transverse Electronic Transport. *Nano Lett.* **2006**, *6* (4), 779–782. https://doi.org/10.1021/nl0601076.
(127) Zwolak, M.; Di Ventra, M. Electronic Signature of DNA Nucleotides *via* Transverse Transport. *Nano Lett.* **2005**, *5* (3), 421–424. https://doi.org/10.1021/nl048289w.
(128) Postma, H. W. Ch. Rapid Sequencing of Individual DNA Molecules in Graphene Nanogaps. *Nano Lett.* **2010**, *10* (2), 420–425. https://doi.org/10.1021/nl9029237.
(129) Traversi, F.; Raillon, C.; Benameur, S. M.; et al. Detecting the Translocation of DNA through a Nanopore Using Graphene Nanoribbons. *Nat. Nanotechnol.* **2013**, *8* (12), 939–945. https://doi.org/10.1038/nnano.2013.240.
(130) Alvarez, J. R.; Skachkov, D.; Massey, S. E.; et al. DNA/RNA Transverse Current Sequencing: Intrinsic Structural Noise from Neighboring Bases. *Front. Genet.* **2015**, *6*, 213. https://doi.org/10.3389/fgene.2015.00213.
(131) Kumawat, R. L.; Jena, M. K.; Mittal, S.; et al. Advancement of Next-Generation DNA Sequencing through Ionic Blockade and Transverse Tunneling Current Methods. *Small* **2024**, *20* (36), 2401112. https://doi.org/10.1002/smll.202401112.
(132) Puster, M.; Balan, A.; Rodríguez-Manzo, J. A.; et al. Cross-Talk Between Ionic and Nanoribbon Current Signals in Graphene Nanoribbon-Nanopore Sensors for Single-Molecule Detection. *Small* **2015**, *11* (47), 6309–6316. https://doi.org/10.1002/smll.201502134.
(133) Lee, C.; Wei, X.; Kysar, J. W.; et al. Measurement of the Elastic Properties and Intrinsic Strength of Monolayer Graphene. *Science* **2008**, *321* (5887), 385–388. https://doi.org/10.1126/science.1157996.
(134) Cao, K.; Feng, S.; Han, Y.; et al. Elastic Straining of Free-Standing Monolayer Graphene. *Nat. Commun.* **2020**, *11* (1), 284. https://doi.org/10.1038/s41467-019-14130-0.
(135) Ghosh, S.; Calizo, I.; Teweldebrhan, D.; et al. Extremely High Thermal Conductivity of Graphene: Prospects for Thermal Management Applications in Nanoelectronic Circuits. *Appl. Phys. Lett.* **2008**, *92* (15), 151911. https://doi.org/10.1063/1.2907977.
(136) Geim, A. K.; Novoselov, K. S. The Rise of Graphene. *Nat. Mater.* **2007**, *6* (3), 183–191. https://doi.org/10.1038/nmat1849.
(137) Wells, D. B.; Belkin, M.; Comer, J.; et al. Assessing Graphene Nanopores for Sequencing DNA. *Nano Lett.* **2012**, *12* (8), 4117–4123. https://doi.org/10.1021/nl301655d.
(138) Heerema, S. J.; Dekker, C. Graphene Nanodevices for DNA Sequencing. *Nat. Nanotechnol.* **2016**, *11* (2), 127–136. https://doi.org/10.1038/nnano.2015.307.
(139) Wasfi, A.; Awwad, F.; Ayesh, A. I. Graphene-Based Nanopore Approaches for DNA Sequencing: A Literature Review. *Biosens. Bioelectron.* **2018**, *119*, 191–203. https://doi.org/10.1016/j.bios.2018.07.072.
(140) Fischbein, M. D.; Drndić, M. Electron Beam Nanosculpting of Suspended Graphene Sheets. *Appl. Phys. Lett.* **2008**, *93* (11), 113107. https://doi.org/10.1063/1.2980518.
(141) Deng, Y.; Huang, Q.; Zhao, Y.; et al. Precise Fabrication of a 5 Nm Graphene Nanopore with a Helium Ion Microscope for Biomolecule Detection. *Nanotechnology* **2016**, *28* (4), 045302. https://doi.org/10.1088/1361-6528/28/4/045302.

(142) Morin, A.; Lucot, D.; Ouerghi, A.; et al. FIB Carving of Nanopores into Suspended Graphene Films. *Microelectron. Eng.* **2012**, *97*, 311–316. https://doi.org/10.1016/j.mee.2012.02.029.
(143) Zandiatashbar, A.; Lee, G.-H.; An, S. J.; et al. Effect of Defects on the Intrinsic Strength and Stiffness of Graphene. *Nat. Commun.* **2014**, *5* (1), 3186. https://doi.org/10.1038/ncomms4186.
(144) Kwok, H.; Briggs, K.; Tabard-Cossa, V. Nanopore Fabrication by Controlled Dielectric Breakdown. *PLOS ONE* **2014**, *9* (3), e92880. https://doi.org/10.1371/journal.pone.0092880.
(145) Dyck, O.; Kim, S.; Kalinin, S. V.; et al. Mitigating E-Beam-Induced Hydrocarbon Deposition on Graphene for Atomic-Scale Scanning Transmission Electron Microscopy Studies. *J. Vac. Sci. Technol. B* **2017**, *36* (1), 011801. https://doi.org/10.1116/1.5003034.
(146) Meyer, J. C.; Girit, C. O.; Crommie, M. F.; et al. Hydrocarbon Lithography on Graphene Membranes. *Appl. Phys. Lett.* **2008**, *92* (12), 123110. https://doi.org/10.1063/1.2901147.
(147) Yang, J.; Ferranti, D. C.; Stern, L. A.; et al. Rapid and Precise Scanning Helium Ion Microscope Milling of Solid-State Nanopores for Biomolecule Detection. *Nanotechnology* **2011**, *22* (28), 285310. https://doi.org/10.1088/0957-4484/22/28/285310.
(148) Kuan, A. T.; Lu, B.; Xie, P.; et al. Electrical Pulse Fabrication of Graphene Nanopores in Electrolyte Solution. *Appl. Phys. Lett.* **2015**, *106* (20), 203109. https://doi.org/10.1063/1.4921620.
(149) Yanagi, I.; Hamamura, H.; Akahori, R.; et al. Two-Step Breakdown of a SiN Membrane for Nanopore Fabrication: Formation of Thin Portion and Penetration. *Sci. Rep.* **2018**, *8* (1), 10129. https://doi.org/10.1038/s41598-018-28524-5.
(150) Su, S.; Wang, X.; Xue, J. Nanopores in Two-Dimensional Materials: Accurate Fabrication. *Mater. Horiz.* **2021**, *8* (5), 1390–1408. https://doi.org/10.1039/D0MH01412E.
(151) Sun, Q.; Dai, M.; Hong, J.; et al. Graphene Nanopore Fabrication and Applications. *Int. J. Mol. Sci.* **2025**, *26* (4), 1709. https://doi.org/10.3390/ijms26041709.
(152) Xie, L.; Jiao, L.; Dai, H. Selective Etching of Graphene Edges by Hydrogen Plasma. *J. Am. Chem. Soc.* **2010**, *132* (42), 14751–14753. https://doi.org/10.1021/ja107071g.
(153) Lee, G.; Cho, K. Electronic Structures of Zigzag Graphene Nanoribbons with Edge Hydrogenation and Oxidation. *Phys. Rev. B* **2009**, *79* (16), 165440. https://doi.org/10.1103/PhysRevB.79.165440.
(154) Simbeck, A. J.; Gu, D.; Kharche, N.; et al. Electronic Structure of Oxygen-Functionalized Armchair Graphene Nanoribbons. *Phys. Rev. B* **2013**, *88* (3), 035413. https://doi.org/10.1103/PhysRevB.88.035413.
(155) Kato, T.; Jiao, L.; Wang, X.; et al. Room-Temperature Edge Functionalization and Doping of Graphene by Mild Plasma. *Small* **2011**, *7* (5), 574–577. https://doi.org/10.1002/smll.201002146.
(156) Baraket, M.; Stine, R.; Lee, W. K.; et al. Aminated Graphene for DNA Attachment Produced *via* Plasma Functionalization. *Appl. Phys. Lett.* **2012**, *100* (23), 233123. https://doi.org/10.1063/1.4711771.
(157) Seitsonen, A. P.; Saitta, A. M.; Wassmann, T.; et al. Structure and Stability of Graphene Nanoribbons in Oxygen, Carbon Dioxide, Water, and Ammonia. *Phys. Rev. B* **2010**, *82* (11), 115425. https://doi.org/10.1103/PhysRevB.82.115425.

(158) Sun, Z.; Kohama, S.; Zhang, Z.; et al. Soluble Graphene through Edge-Selective Functionalization. *Nano Res.* **2010**, *3* (2), 117–125. https://doi.org/10.1007/s12274-010-1016-2.
(159) Sharma, R.; Baik, J. H.; Perera, C. J.; et al. Anomalously Large Reactivity of Single Graphene Layers and Edges toward Electron Transfer Chemistries. *Nano Lett.* **2010**, *10* (2), 398–405. https://doi.org/10.1021/nl902741x.
(160) Bellunato, A.; Schneider, G. F. Electrophilic Radical Coupling at the Edge of Graphene. *Nanoscale* **2018**, *10* (25), 12011–12017. https://doi.org/10.1039/C8NR03429J.
(161) Zhuang, B.; Li, S.; Li, S.; et al. Ways to Eliminate PMMA Residues on Graphene — — Superclean Graphene. *Carbon* **2021**, *173*, 609–636. https://doi.org/10.1016/j.carbon.2020.11.047.
(162) Pirkle, A.; Chan, J.; Venugopal, A.; et al. The Effect of Chemical Residues on the Physical and Electrical Properties of Chemical Vapor Deposited Graphene Transferred to SiO2. *Appl. Phys. Lett.* **2011**, *99* (12), 122108. https://doi.org/10.1063/1.3643444.
(163) Paulus, G. L. C.; Wang, Q. H.; Strano, M. S. Covalent Electron Transfer Chemistry of Graphene with Diazonium Salts. *Acc. Chem. Res.* **2013**, *46* (1), 160–170. https://doi.org/10.1021/ar300119z.
(164) Iqbal, M. W.; Iqbal, M. Z.; Jin, X.; et al. Edge Oxidation Effect of Chemical-Vapor-Deposition-Grown Graphene Nanoconstriction. *ACS Appl. Mater. Interfaces* **2014**, *6* (6), 4207–4213. https://doi.org/10.1021/am405885c.
(165) Eckmann, A.; Felten, A.; Mishchenko, A.; et al. Probing the Nature of Defects in Graphene by Raman Spectroscopy. *Nano Lett.* **2012**, *12* (8), 3925–3930. https://doi.org/10.1021/nl300901a.
(166) Lucchese, M. M.; Stavale, F.; Ferreira, E. H. M.; et al. Quantifying Ion-Induced Defects and Raman Relaxation Length in Graphene. *Carbon* **2010**, *48* (5), 1592–1597. https://doi.org/10.1016/j.carbon.2009.12.057.
(167) Ferrari, A. C.; Basko, D. M. Raman Spectroscopy as a Versatile Tool for Studying the Properties of Graphene. *Nat. Nanotechnol.* **2013**, *8* (4), 235–246. https://doi.org/10.1038/nnano.2013.46.
(168) Friedbacher, G.; Bubert, H. *Surface and Thin Film Analysis: A Compendium of Principles, Instrumentation, and Applications*; John Wiley & Sons, **2011**.
(169) Kisielowski, C.; Freitag, B.; Bischoff, M.; et al. Detection of Single Atoms and Buried Defects in Three Dimensions by Aberration-Corrected Electron Microscope with 0.5-Å Information Limit. *Microsc. Microanal.* **2008**, *14* (5), 469–477. https://doi.org/10.1017/S1431927608080902.
(170) Kelly, D. J.; Zhou, M.; Clark, N.; et al. Nanometer Resolution Elemental Mapping in Graphene-Based TEM Liquid Cells. *Nano Lett.* **2018**, *18* (2), 1168–1174. https://doi.org/10.1021/acs.nanolett.7b04713.
(171) Suenaga, K.; Tencé, M.; Mory, C.; et al. Element-Selective Single Atom Imaging. *Science* **2000**, *290* (5500), 2280–2282. https://doi.org/10.1126/science.290.5500.2280.
(172) Cai, J.; Ruffieux, P.; Jaafar, R.; et al. Atomically Precise Bottom-up Fabrication of Graphene Nanoribbons. *Nature* **2010**, *466* (7305), 470–473. https://doi.org/10.1038/nature09211.

(173) Zhang, X.; Yazyev, O. V.; Feng, J.; et al. Experimentally Engineering the Edge Termination of Graphene Nanoribbons. *ACS Nano* **2013**, *7* (1), 198–202. https://doi.org/10.1021/nn303730v.
(174) Lee, J. U.; Lee, W.; Yoon, S. S.; et al. Site-Selective Immobilization of Gold Nanoparticles on Graphene Sheets and Its Electrochemical Properties. *Appl. Surf. Sci.* **2014**, *315*, 73–80. https://doi.org/10.1016/j.apsusc.2014.07.099.
(175) Can, B. S. Chemistry and Characterization of the Graphene Basal Plane and Edge for Recognition Tunneling, Leiden University, **2025**. https://hdl.handle.net/1887/4245957 (accessed 2025-09-24).
(176) Georgakilas, V.; Tiwari, J. N.; Kemp, K. C.; et al. Noncovalent Functionalization of Graphene and Graphene Oxide for Energy Materials, Biosensing, Catalytic, and Biomedical Applications. *Chem. Rev.* **2016**, *116* (9), 5464–5519. https://doi.org/10.1021/acs.chemrev.5b00620.
(177) Georgakilas, V.; Otyepka, M.; Bourlinos, A. B.; et al. Functionalization of Graphene: Covalent and Non-Covalent Approaches, Derivatives and Applications. *Chem. Rev.* **2012**, *112* (11), 6156–6214. https://doi.org/10.1021/cr3000412.
(178) Lehn, J. M. *Supramolecular Chemistry: Concepts and Perspectives*; Wiley-VCH: Weinheim, **1995**. https://doi.org/10.1002/3527607439.fmatter.
(179) Crowley, P. B. Origins of the Host–Guest Terminology. *Cryst. Growth Des.* **2023**, *23* (12), 8469–8473. https://doi.org/10.1021/acs.cgd.3c00985.
(180) Lehn, J. M. Cryptates: The Chemistry of Macropolycyclic Inclusion Complexes. *Acc. Chem. Res.* **1978**, *11* (2), 49–57. https://doi.org/10.1021/ar50122a001.
(181) Cram, D. J.; Kaneda, T.; Helgeson, R. C.; et al. Host-Guest Complexation. 35. Spherands, the First Completely Preorganized Ligand Systems. *J. Am. Chem. Soc.* **1985**, *107* (12), 3645–3657. https://doi.org/10.1021/ja00298a040.
(182) Zhang, M.; Yan, X.; Huang, F.; et al. Stimuli-Responsive Host–Guest Systems Based on the Recognition of Cryptands by Organic Guests. *Acc. Chem. Res.* **2014**, *47* (7), 1995–2005. https://doi.org/10.1021/ar500046r.
(183) Pan, Y.-C.; Tian, J.-H.; Guo, D.-S. Molecular Recognition with Macrocyclic Receptors for Application in Precision Medicine. *Acc. Chem. Res.* **2023**, *56* (24), 3626–3639. https://doi.org/10.1021/acs.accounts.3c00585.
(184) Li, Z.; Han, Y.; Gao, Z.; et al. Supramolecular Engineering of Discrete Pt(II)···Pt(II) Interactions for Visible-Light Photocatalysis. *ACS Catal.* **2017**, *7* (7), 4676–4681. https://doi.org/10.1021/acscatal.7b00709.
(185) Yuan, M.; Zhang, X.; Han, Y.; et al. Organoplatinum(II)-Based Self-Complementary Molecular Tweezers with Guest-Induced Fluorochromic Behaviors. *Inorg. Chem.* **2020**, *59* (19), 14134–14140. https://doi.org/10.1021/acs.inorgchem.0c01899.
(186) Tian, Y.-K.; Shi, Y.-G.; Yang, Z.-S.; et al. Responsive Supramolecular Polymers Based on the Bis[Alkynylplatinum(II)] Terpyridine Molecular Tweezer/Arene Recognition Motif. *Angew. Chem.* **2014**, *126* (24), 6204–6208. https://doi.org/10.1002/ange.201402192.
(187) de Jong, J.; Bos, J. E.; Wezenberg, S. J. Stimulus-Controlled Anion Binding and Transport by Synthetic Receptors. *Chem. Rev.* **2023**, *123* (13), 8530–8574. https://doi.org/10.1021/acs.chemrev.3c00039.
(188) Klärner, F.-G.; Schrader, T. Aromatic Interactions by Molecular Tweezers and Clips in Chemical and Biological Systems. *Acc. Chem. Res.* **2013**, *46* (4), 967–978. https://doi.org/10.1021/ar300061c.

(189) Zhang, X.; Han, Y.; Liu, G.; et al. Macrocyclic *versus* Acyclic Preorganization in Organoplatinum(II)-Based Host–guest Complexes. *Chin. Chem. Lett.* **2019**, *30* (11), 1927–1930. https://doi.org/10.1016/j.cclet.2019.05.007.
(190) Hardouin–Lerouge, M.; Hudhomme, P.; Sallé, M. Molecular Clips and Tweezers Hosting Neutral Guests. *Chem. Soc. Rev.* **2011**, *40* (1), 30–43. https://doi.org/10.1039/B915145C.
(191) Han, Y.; Tian, Y.; Li, Z.; et al. Donor–Acceptor-Type Supramolecular Polymers on the Basis of Preorganized Molecular Tweezers/Guest Complexation. *Chem. Soc. Rev.* **2018**, *47* (14), 5165–5176. https://doi.org/10.1039/C7CS00802C.
(192) Tian, Y.-K.; Han, Y.-F.; Yang, Z.-S.; et al. Donor–Acceptor-Type Supramolecular Polymers Derived from Robust yet Responsive Heterodimeric Tweezers. *Macromolecules* **2016**, *49* (17), 6455–6461. https://doi.org/10.1021/acs.macromol.6b01032.
(193) Mbarek, A.; Moussa, G.; Leblond Chain, J. Pharmaceutical Applications of Molecular Tweezers, Clefts and Clips. *Molecules* **2019**, *24* (9), 1803. https://doi.org/10.3390/molecules24091803.
(194) Chen, C. W.; Whitlock, H. W. Jr. Molecular Tweezers: A Simple Model of Bifunctional Intercalation. *J. Am. Chem. Soc.* **1978**, *100* (15), 4921–4922. https://doi.org/10.1021/ja00483a063.
(195) Biz, C.; Ibáñez, S.; Poyatos, M.; et al. Gold(I) Metallo-Tweezers for the Recognition of Functionalized Polycyclic Aromatic Hydrocarbons by Combined π–π Stacking and H-Bonding. *Chem. – Eur. J.* **2017**, *23* (58), 14439–14444. https://doi.org/10.1002/chem.201703984.
(196) Cram, D. J. The Design of Molecular Hosts, Guests, and Their Complexes. *Science* **1988**, *240* (4853), 760–767. https://doi.org/10.1126/science.3283937.
(197) Petitjean, A.; Khoury, R. G.; Kyritsakas, N.; et al. Dynamic Devices. Shape Switching and Substrate Binding in Ion-Controlled Nanomechanical Molecular Tweezers. *J. Am. Chem. Soc.* **2004**, *126* (21), 6637–6647. https://doi.org/10.1021/ja031915r.
(198) Doistau, B.; Rossi-Gendron, C.; Tron, A.; et al. Switchable Platinum-Based Tweezers with Pt–Pt Bonding and Selective Luminescence Quenching. *Dalton Trans.* **2015**, *44* (18), 8543–8551. https://doi.org/10.1039/C4DT03230F.
(199) Benda, L.; Doistau, B.; Hasenknopf, B.; et al. Synthesis and Guest Recognition of Switchable Pt-Salphen Based Molecular Tweezers. *Molecules* **2018**, *23* (5), 990. https://doi.org/10.3390/molecules23050990.
(200) Doistau, B.; Benda, L.; Cantin, J.-L.; et al. Six States Switching of Redox-Active Molecular Tweezers by Three Orthogonal Stimuli. *J. Am. Chem. Soc.* **2017**, *139* (27), 9213–9220. https://doi.org/10.1021/jacs.7b02945.
(201) Fokkens, M.; Schrader, T.; Klärner, F.-G. A Molecular Tweezer for Lysine and Arginine. *J. Am. Chem. Soc.* **2005**, *127* (41), 14415–14421. https://doi.org/10.1021/ja052806a.
(202) Plante, J. P.; Glass, T. E. Shape-Selective Fluorescent Sensing Ensemble Using a Tweezer-Type Metalloreceptor. *Org. Lett.* **2006**, *8* (10), 2163–2166. https://doi.org/10.1021/ol060641k.
(203) Banerjee, S.; Veale, E. B.; Phelan, C. M.; et al. Recent Advances in the Development of 1,8-Naphthalimide Based DNA Targeting Binders, Anticancer and Fluorescent Cellular Imaging Agents. *Chem. Soc. Rev.* **2013**, *42* (4), 1601–1618. https://doi.org/10.1039/C2CS35467E.

(204) Kirupakaran, A.; van den Boom, J.; Blueggel, M.; et al. Molecular Tweezers Block the Functional Pore of a Protein Machine. *J. Am. Chem. Soc.* **2025**, *147* (20), 16836–16849. https://doi.org/10.1021/jacs.4c15288.
(205) Schrader, T.; Bitan, G.; Klärner, F.-G. Molecular Tweezers for Lysine and Arginine – Powerful Inhibitors of Pathologic Protein Aggregation. *Chem. Commun.* **2016**, *52* (76), 11318–11334. https://doi.org/10.1039/C6CC04640A.
(206) Hardy, J.; Selkoe, D. J. The Amyloid Hypothesis of Alzheimer's Disease: Progress and Problems on the Road to Therapeutics. *Science* **2002**, *297* (5580), 353–356. https://doi.org/10.1126/science.1072994.
(207) Herrera-Vaquero, M.; Bouquio, D.; Kallab, M.; et al. The Molecular Tweezer CLR01 Reduces Aggregated, Pathologic, and Seeding-Competent α-Synuclein in Experimental Multiple System Atrophy. *Biochim. Biophys. Acta BBA - Mol. Basis Dis.* **2019**, *1865* (11), 165513. https://doi.org/10.1016/j.bbadis.2019.07.007.
(208) Monaco, A.; Maffia, V.; Sorrentino, N. C.; et al. The Amyloid Inhibitor CLR01 Relieves Autophagy and Ameliorates Neuropathology in a Severe Lysosomal Storage Disease. *Mol. Ther.* **2020**, *28* (4), 1167–1176. https://doi.org/10.1016/j.ymthe.2020.02.005.
(209) Gao, Z.; Han, Y.; Gao, Z.; et al. Multicomponent Assembled Systems Based on Platinum(II) Terpyridine Complexes. *Acc. Chem. Res.* **2018**, *51* (11), 2719–2729. https://doi.org/10.1021/acs.accounts.8b00340.
(210) Ibáñez, S.; Peris, E. Shape-Adaptability and Redox-Switching Properties of a Di-Gold Metallotweezer. *Chem. – Eur. J.* **2021**, *27* (37), 9661–9665. https://doi.org/10.1002/chem.202100794.
(211) Tanaka, Y.; Wong, K. M.-C.; Yam, V. W.-W. Host–Guest Interactions of Phosphorescent Molecular Tweezers Based on an Alkynylplatinum(II) Terpyridine System with Polyaromatic Hydrocarbons. *Chem. – Eur. J.* **2013**, *19* (1), 390–399. https://doi.org/10.1002/chem.201201942.
(212) Ibáñez, S.; Peris, E. "Lock and Key" and "Induced-Fit" Host–Guest Models in Two Digold(I)-Based Metallotweezers. *Inorg. Chem.* **2023**, *62* (5), 1820–1826. https://doi.org/10.1021/acs.inorgchem.2c00677.
(213) Ibáñez, S. The New Di-Gold Metallotweezer Based on an Alkynylpyridine System. *Molecules* **2022**, *27* (12), 3699. https://doi.org/10.3390/molecules27123699.
(214) Ibáñez, S.; Vicent, C.; Peris, E. Clippane: A Mechanically Interlocked Molecule (MIM) Based on Molecular Tweezers. *Angew. Chem. Int. Ed.* **2022**, *61* (2), e202112513. https://doi.org/10.1002/anie.202112513.
(215) Ren, J.; Jiang, S.; Han, T.; et al. Dual Supramolecular Chirogenesis Based on Platinum(II) Metallotweezers. *Chem. Commun.* **2023**, *59* (6), 744–747. https://doi.org/10.1039/D2CC05787E.
(216) Gao, Z.; Tian, Y.; Hsu, H.-K.; et al. Additive-Controlled Kinetic Trapping of Quadruple Platinum(II) Stacks with Emergent Photothermal Behaviors. *CCS Chem.* **2021**, *3* (10), 105–115. https://doi.org/10.31635/ccschem.021.202000511.
(217) Tanaka, Y.; Wong, K. M.-C.; Yam, V. W.-W. Platinum-Based Phosphorescent Double-Decker Tweezers: A Strategy for Extended Heterologous Metal–Metal Interactions. *Angew. Chem. Int. Ed.* **2013**, *52* (52), 14117–14120. https://doi.org/10.1002/anie.201306025.
(218) Kong, F. K.-W.; Chan, A. K.-W.; Ng, M.; et al. Construction of Discrete Pentanuclear Platinum(II) Stacks with Extended Metal–Metal Interactions by Using

Phosphorescent Platinum(II) Tweezers. *Angew. Chem. Int. Ed.* **2017**, *56* (47), 15103–15107. https://doi.org/10.1002/anie.201708504.

(219) Msellem, P.; Dekthiarenko, M.; Seyd, N. H.; et al. Switchable Molecular Tweezers: Design and Applications. *Beilstein J. Org. Chem.* **2024**, *20* (1), 504–539. https://doi.org/10.3762/bjoc.20.45.

(220) Zimmerman, S. C. Rigid Molecular Tweezers as Hosts for the Complexation of Neutral Guests. In *Supramolecular Chemistry I — Directed Synthesis and Molecular Recognition*; Eds.; Springer: Berlin, Heidelberg, **1993**; pp 71–102.

(221) Vafakish, B.; Wilson, L. D. Supramolecular Chemistry of Polymer-Based Molecular Tweezers: A Minireview. *Surfaces* **2024**, *7* (3), 752–769. https://doi.org/10.3390/surfaces7030049.

(222) Doistau, B.; Tron, A.; Denisov, S. A.; et al. Terpy(Pt–Salphen)2 Switchable Luminescent Molecular Tweezers. *Chem. – Eur. J.* **2014**, *20* (48), 15799–15807. https://doi.org/10.1002/chem.201404064.

(223) Li, Z.; Han, Y.; Gao, Z.; et al. Non-Covalent Molecular Tweezer/Guest Complexation with Pt(II)···Pt(II) Metal–Metal Interactions: Toward Intelligent Photocatalytic Materials. *Mater. Chem. Front.* **2017**, *2* (1), 76–80. https://doi.org/10.1039/C7QM00424A.

(224) Lv, X.; Han, Y.; Yang, Z.; et al. Pre-Organized Molecular Tweezer Stabilized by Intramolecular Hydrogen Bonds: Solvent-Responsive Host–Guest Complexation. *Tetrahedron Lett.* **2016**, *57* (18), 1971–1975. https://doi.org/10.1016/j.tetlet.2016.03.080.

(225) Fu, T.; Li, Z.; Zhang, Z.; et al. Supramolecular Cross-Linking and Gelation of Conjugated Polycarbazoles *via* Hydrogen Bond Assisted Molecular Tweezer/Guest Complexation. *Macromolecules* **2017**, *50* (19), 7517–7525. https://doi.org/10.1021/acs.macromol.7b01149.

(226) Gao, Z.; Han, Y.; Chen, J.; et al. Trimethylammonium-Derived Molecular Tweezers and Their Host–Guest Complexation Behaviours in Polar Media. *Chem. – Asian J.* **2016**, *11* (12), 1775–1779. https://doi.org/10.1002/asia.201600364.

(227) Zhang, X.; Ao, L.; Han, Y.; et al. Modulating Pt···Pt Metal–Metal Interactions through Conformationally Switchable Molecular Tweezer/Guest Complexation. *Chem. Commun.* **2018**, *54* (14), 1754–1757. https://doi.org/10.1039/C8CC00216A.

(228) Gosset, A.; Xu, Z.; Maurel, F.; et al. A Chemically-Responsive Bis-Acridinium Receptor. *New J. Chem.* **2018**, *42* (6), 4728–4734. https://doi.org/10.1039/C7NJ03712K.

(229) Tanaka, Y.; Wong, K. M.-C.; Yam, V. W.-W. Phosphorescent Molecular Tweezers Based on Alkynylplatinum(II) Terpyridine System: Turning on of NIR Emission *via* Heterologous Pt···M Interactions (M = PtII, PdII, AuIII and AuI). *Chem. Sci.* **2012**, *3* (4), 1185–1191. https://doi.org/10.1039/C2SC00935H.

(230) Zhong, H.; Jiang, S.; Ao, L.; et al. Phosphorescent Host–Guest Complexes on the Basis of Polyhedral Oligomeric Silsesquioxane-Functionalized Metallotweezers. *Inorg. Chem.* **2022**, *61* (18), 7111–7119. https://doi.org/10.1021/acs.inorgchem.2c00340.

(231) Nabeshima, T.; Hasegawa, Y.; Trokowski, R.; et al. Synthesis and Guest Recognition of Molecular Cleft Consisting of Terpyridine–Pt(II) Acetylide Complexes. *Tetrahedron Lett.* **2012**, *53* (46), 6182–6185. https://doi.org/10.1016/j.tetlet.2012.08.116.

(232) Leblond, J.; Petitjean, A. Molecular Tweezers: Concepts and Applications. *ChemPhysChem* **2011**, *12* (6), 1043–1051. https://doi.org/10.1002/cphc.201001050.
(233) Li, Z.; Han, Y.; Jin, F.; et al. Bis[Alkynylplatinum(II)] Terpyridine Molecular Tweezer with Conformationally-Rigid Spacer: Modulating the Binding Selectivity in a Three-Component Supramolecular Recognition System. *Dalton Trans.* **2016**, *45* (43), 17290–17295. https://doi.org/10.1039/C6DT03160A.
(234) Goto, Y.; Haga, T.; Yanagi, I.; et al. Deceleration of Single-Stranded DNA Passing through a Nanopore Using a Nanometre-Sized Bead Structure. *Sci. Rep.* **2015**, *5* (1), 16640. https://doi.org/10.1038/srep16640.
(235) Menanteau, T.; Dias, M.; Levillain, E.; et al. Electrografting *via* Diazonium Chemistry: The Key Role of the Aryl Substituent in the Layer Growth Mechanism. *J. Phys. Chem. C* **2016**, *120* (8), 4423–4429. https://doi.org/10.1021/acs.jpcc.5b12565.
(236) Tahara, K.; Kubo, Y.; Lindner, B.; et al. Steric and Electronic Effects of Electrochemically Generated Aryl Radicals on Grafting of the Graphite Surface. *Langmuir* **2019**, *35* (6), 2089–2098. https://doi.org/10.1021/acs.langmuir.8b03339.
(237) Trung Huynh, T. M.; Tahara, K.; Feyter, S. D.; et al. On the Role of Functional Groups in the Formation of Diazonium Based Covalent Attachments: Dendritic vs. Layer-by-Layer Growth. *RSC Adv.* **2023**, *13* (35), 24576–24582. https://doi.org/10.1039/D3RA02661B.
(238) Gu, Y.; Qiu, Z.; Müllen, K. Nanographenes and Graphene Nanoribbons as Multitalents of Present and Future Materials Science. *J. Am. Chem. Soc.* **2022**, *144* (26), 11499–11524. https://doi.org/10.1021/jacs.2c02491.
(239) Müllen, K.; Rabe, J. P. Nanographenes as Active Components of Single-Molecule Electronics and How a Scanning Tunneling Microscope Puts Them To Work. *Acc. Chem. Res.* **2008**, *41* (4), 511–520. https://doi.org/10.1021/ar7001446.
(240) Paternò, G. M.; Goudappagouda; Chen, Q.; et al. Large Polycyclic Aromatic Hydrocarbons as Graphene Quantum Dots: From Synthesis to Spectroscopy and Photonics. *Adv. Opt. Mater.* **2021**, *9* (23), 2100508. https://doi.org/10.1002/adom.202100508.
(241) Daría, A. M. S.; González-Sánchez, L.; Gómez, S. Coronene: A Model for Ultrafast Dynamics in Graphene Nanoflakes and PAHs. *Phys. Chem. Chem. Phys.* **2023**, *26* (1), 174–184. https://doi.org/10.1039/D3CP03656A.
(242) Rieger, R.; Müllen, K. Forever Young: Polycyclic Aromatic Hydrocarbons as Model Cases for Structural and Optical Studies. *J. Phys. Org. Chem.* **2010**, *23* (4), 315–325. https://doi.org/10.1002/poc.1644.
(243) Reichardt, C.; Welton, T. *Solvents and Solvent Effects in Organic Chemistry*; John Wiley & Sons, **2011**.
(244) Kanagaraj, K.; Alagesan, M.; Inoue, Y.; et al. 1.02 - Solvation Effects in Supramolecular Chemistry. In *Comprehensive Supramolecular Chemistry II*; Atwood, J. L., Ed.; Elsevier: Oxford, **2017**; pp 11–60. https://doi.org/10.1016/B978-0-12-409547-2.12481-3.
(245) Menschutkin, N. Über die Affinitätskoeffizienten der Alkylhaloide und der Amine: Zweiter Teil. Über den Einfluss des chemisch indifferenten flüssigen Mediums auf die Geschwindigkeit der Verbindung des Triäthylamins mit den Alkyljodiden. *Z. Für Phys. Chem.* **1890**, *6U* (1), 41–57. https://doi.org/10.1515/zpch-1890-0607.
(246) Reichardt, C. Solvation Effects in Organic Chemistry: A Short Historical Overview. *J. Org. Chem.* **2022**, *87* (3), 1616–1629. https://doi.org/10.1021/acs.joc.1c01979.

(247) Burrows, C. J.; Harper, J. B.; Sander, W.; et al. Solvation Effects in Organic Chemistry. *J. Org. Chem.* **2022**, *87* (3), 1599–1601. https://doi.org/10.1021/acs.joc.1c03148.
(248) Muller, P. Glossary of Terms Used in Physical Organic Chemistry (IUPAC Recommendations 1994). *Pure Appl. Chem.* **1994**, *66* (5), 1077–1184. https://doi.org/10.1351/pac199466051077.
(249) Tielrooij, K. J.; Garcia-Araez, N.; Bonn, M.; et al. Cooperativity in Ion Hydration. *Science* **2010**, *328* (5981), 1006–1009. https://doi.org/10.1126/science.1183512.
(250) Yoshizawa, M.; Kusukawa, T.; Kawano, M.; et al. Endohedral Clusterization of Ten Water Molecules into a "Molecular Ice" within the Hydrophobic Pocket of a Self-Assembled Cage. *J. Am. Chem. Soc.* **2005**, *127* (9), 2798–2799. https://doi.org/10.1021/ja043953w.
(251) Koga, K.; Gao, G. T.; Tanaka, H.; et al. Formation of Ordered Ice Nanotubes inside Carbon Nanotubes. *Nature* **2001**, *412* (6849), 802–805. https://doi.org/10.1038/35090532.
(252) Ewing, M. B.; Lilley, T. H.; Olofsson, G. M.; et al. Standard Quantities in Chemical Thermodynamics. Fugacities, Activities and Equilibrium Constants for Pure and Mixed Phases (IUPAC Recommendations 1994). *Pure Appl. Chem.* **1994**, *66* (3), 533–552. https://doi.org/10.1351/pac199466030533.
(253) Chapman, K. T.; Still, W. C. A Remarkable Effect of Solvent Size on the Stability of a Molecular Complex. *J. Am. Chem. Soc.* **1989**, *111* (8), 3075–3077.
(254) Würthner, F. Solvent Effects in Supramolecular Chemistry: Linear Free Energy Relationships for Common Intermolecular Interactions. *J. Org. Chem.* **2022**, *87* (3), 1602–1615. https://doi.org/10.1021/acs.joc.1c00625.
(255) Sherbow, T. J.; Fargher, H. A.; Haley, M. M.; et al. Solvent-Dependent Linear Free-Energy Relationship in a Flexible Host–Guest System. *J. Org. Chem.* **2020**, *85* (19), 12367–12373. https://doi.org/10.1021/acs.joc.0c01616.
(256) Smithrud, D. B.; Sanford, E. M.; Chao, I.; et al. Solvent Effects in Molecular Recognition. *Pure Appl. Chem.* **1990**, *62* (12), 2227–2236. https://doi.org/10.1351/pac199062122227.
(257) Smithrud, D. B.; Diederich, F. Strength of Molecular Complexation of Apolar Solutes in Water and in Organic Solvents Is Predictable by Linear Free Energy Relationships: A General Model for Solvation Effects on Apolar Binding. *J. Am. Chem. Soc.* **1990**, *112* (1), 339–343. https://doi.org/10.1021/ja00157a052.
(258) Cubberley, M. S.; Iverson, B. L. 1H NMR Investigation of Solvent Effects in Aromatic Stacking Interactions. *J. Am. Chem. Soc.* **2001**, *123* (31), 7560–7563. https://doi.org/10.1021/ja015817m.
(259) Mizutani, T.; Wada, K.; Kitagawa, S. Molecular Recognition of Amines and Amino Esters by Zinc Porphyrin Receptors: Binding Mechanisms and Solvent Effects. *J. Org. Chem.* **2000**, *65* (19), 6097–6106. https://doi.org/10.1021/jo000557x.
(260) Chen, Z.; Fimmel, B.; Würthner, F. Solvent and Substituent Effects on Aggregation Constants of Perylene Bisimide π-Stacks – a Linear Free Energy Relationship Analysis. *Org. Biomol. Chem.* **2012**, *10* (30), 5845–5855. https://doi.org/10.1039/C2OB07131B.
(261) Solov'ev, V. P.; Strakhova, N. N.; Raevsky, O. A.; et al. Solvent Effects on Crown Ether Complexations. *J. Org. Chem.* **1996**, *61* (16), 5221–5226. https://doi.org/10.1021/jo952250h.

(262) Spange, S.; Weiß, N.; Schmidt, C. H.; et al. Reappraisal of Empirical Solvent Polarity Scales for Organic Solvents. *Chemistry–Methods* **2021**, *1* (1), 42–60. https://doi.org/10.1002/cmtd.202000039.
(263) RosCs, M.; Rafols, C.; Ortega, J.; et al. Solute-Solvent and Solvent-Solvent Interactions in Binary Solvent Mixtures. Part 1. A Comparison of Several Preferential Solvation Models for Describing ET (30) Polarity of Dipolar Hydrogen Bond Acceptor-Cosolvent Mixtures. *J. Chem. Soc. Perkin Trans. 2* **1995**.
(264) Katritzky, A. R.; Fara, D. C.; Yang, H.; et al. Quantitative Measures of Solvent Polarity. *Chem. Rev.* **2004**, *104* (1), 175–198. https://doi.org/10.1021/cr020750m.
(265) Erchinger, J. E.; Okumura, T.; Nakata, K.; et al. Functionalization and Solubilization of Polycyclic Aromatic Compounds by Sulfoniumization. *Chem. Sci.* **2025**, *16* (19), 8262–8267. https://doi.org/10.1039/D5SC01415H.
(266) Yang, W.; Lucotti, A.; Tommasini, M.; et al. Bottom-Up Synthesis of Soluble and Narrow Graphene Nanoribbons Using Alkyne Benzannulations. *J. Am. Chem. Soc.* **2016**, *138* (29), 9137–9144. https://doi.org/10.1021/jacs.6b03014.
(267) Wong, W. W. H.; Jones, D. J.; Yan, C.; et al. Synthesis, Photophysical, and Device Properties of Novel Dendrimers Based on a Fluorene−Hexabenzocoronene (FHBC) Core. *Org. Lett.* **2009**, *11* (4), 975–978. https://doi.org/10.1021/ol8029164.
(268) Feng, X.; Pisula, W.; Müllen, K. Large Polycyclic Aromatic Hydrocarbons: Synthesis and Discotic Organization. *Pure Appl. Chem.* **2009**, *81* (12), 2203–2224. https://doi.org/10.1351/PAC-CON-09-07-07.
(269) Souza, F. P. S.; Heinzelmann, G.; Caramori, G. F. Investigating the Solvent Effects on Binding Affinity of PAHs–ExBox4+ Complexes: An Alchemical Approach. *J. Phys. Chem. B* **2023**, *127* (1), 249–260. https://doi.org/10.1021/acs.jpcb.2c06271.
(270) Merino, G.; Solà, M.; Fernández, I.; et al. Aromaticity: Quo Vadis. *Chem. Sci.* **2023**, *14* (21), 5569–5576. https://doi.org/10.1039/D2SC04998H.
(271) Chemistry (IUPAC), T. I. U. of P. and A. *IUPAC - aromaticity (A00442)*. https://doi.org/10.1351/goldbook.A00442.
(272) Hückel, E. Quanstentheoretische Beiträge zum Benzolproblem. *Z. Für Phys.* **1931**, *72* (5), 310–337. https://doi.org/10.1007/BF01341953.
(273) Hückel, E. Quantentheoretische Beiträge zum Benzolproblem. *Z. Für Phys.* **1931**, *70* (3), 204–286. https://doi.org/10.1007/BF01339530.
(274) Hückel, E. Quantentheoretische Beiträge zum Problem der aromatischen und ungesättigten Verbindungen. III. *Z. Für Phys.* **1932**, *76* (9), 628–648. https://doi.org/10.1007/BF01341936.
(275) Randić, M. Aromaticity of Polycyclic Conjugated Hydrocarbons. *Chem. Rev.* **2003**, *103* (9), 3449–3606. https://doi.org/10.1021/cr9903656.
(276) Galabov, B.; Ilieva, S.; Cheshmedzhieva, D.; et al. Mini-Review on Structure–Reactivity Relationship for Aromatic Molecules: Recent Advances. *ACS Omega* **2022**, *7* (10), 8199–8208. https://doi.org/10.1021/acsomega.1c07176.
(277) Gershoni-Poranne, R.; Stanger, A. Magnetic Criteria of Aromaticity. *Chem. Soc. Rev.* **2015**, *44* (18), 6597–6615. https://doi.org/10.1039/C5CS00114E.
(278) Mallah, M. A.; Changxing, L.; Mallah, M. A.; et al. Polycyclic Aromatic Hydrocarbon and Its Effects on Human Health: An Overeview. *Chemosphere* **2022**, *296*, 133948. https://doi.org/10.1016/j.chemosphere.2022.133948.
(279) Venkatraman, G.; Giribabu, N.; Mohan, P. S.; et al. Environmental Impact and Human Health Effects of Polycyclic Aromatic Hydrocarbons and Remedial

Strategies: A Detailed Review. *Chemosphere* **2024**, *351*, 141227. https://doi.org/10.1016/j.chemosphere.2024.141227.
(280) Feng, Y.; Li, Z.; Li, W. Polycyclic Aromatic Hydrocarbons (PAHs): Environmental Persistence and Human Health Risks. *Nat. Prod. Commun.* **2025**, *20* (1), 1934578X241311451. https://doi.org/10.1177/1934578X241311451.
(281) Baird, W. M.; Hooven, L. A.; Mahadevan, B. Carcinogenic Polycyclic Aromatic Hydrocarbon-DNA Adducts and Mechanism of Action. *Environ. Mol. Mutagen.* **2005**, *45* (2–3), 106–114. https://doi.org/10.1002/em.20095.
(282) Sekar, M.; T R, P. Critical Review on the Formations and Exposure of Polycyclic Aromatic Hydrocarbons (PAHs) in the Conventional Hydrocarbon-Based Fuels: Prevention and Control Strategies. *Chemosphere* **2024**, *350*, 141005. https://doi.org/10.1016/j.chemosphere.2023.141005.
(283) Phillips, D. H. Polycyclic Aromatic Hydrocarbons in the Diet. *Mutat. Res. Toxicol. Environ. Mutagen.* **1999**, *443* (1), 139–147. https://doi.org/10.1016/S1383-5742(99)00016-2.
(284) Cami, J.; Bernard-Salas, J.; Peeters, E.; et al. Detection of C60 and C70 in a Young Planetary Nebula. *Science* **2010**, *329* (5996), 1180–1182. https://doi.org/10.1126/science.1192035.
(285) Salama, F. PAHs in Astronomy - A Review. *Proc. Int. Astron. Union* **2008**, *4* (S251), 357–366. https://doi.org/10.1017/S1743921308021960.
(286) Li, A. Spitzer's Perspective of Polycyclic Aromatic Hydrocarbons in Galaxies. *Nat. Astron.* **2020**, *4* (4), 339–351. https://doi.org/10.1038/s41550-020-1051-1.
(287) Hrodmarsson, H. R.; Aleman, I.; Candian, A.; et al. The AstroPAH 10 Years of Science Review. *Space Sci. Rev.* **2025**, *221* (4), 42. https://doi.org/10.1007/s11214-025-01161-x.
(288) Ehrenfreund, P.; Rasmussen, S.; Cleaves, J.; et al. Experimentally Tracing the Key Steps in the Origin of Life: The Aromatic World. *Astrobiology* **2006**, *6* (3), 490–520. https://doi.org/10.1089/ast.2006.6.490.
(289) Li, Q.; Zhang, Y.; Xie, Z.; et al. Polycyclic Aromatic Hydrocarbon-Based Organic Semiconductors: Ring-Closing Synthesis and Optoelectronic Properties. *J. Mater. Chem. C* **2022**, *10* (7), 2411–2430. https://doi.org/10.1039/D1TC04866J.
(290) Delouche, T.; Hissler, M.; Bouit, P.-A. Polycyclic Aromatic Hydrocarbons Containing Heavy Group 14 Elements: From Synthetic Challenges to Optoelectronic Devices. *Coord. Chem. Rev.* **2022**, *464*, 214553. https://doi.org/10.1016/j.ccr.2022.214553.
(291) Zhang, Z.; Zhang, Q. Recent Progress in Well-Defined Higher Azaacenes ($n \geq 6$): Synthesis, Molecular Packing, and Applications. *Mater. Chem. Front.* **2020**, *4* (12), 3419–3432. https://doi.org/10.1039/C9QM00656G.
(292) Wang, C.; Dong, H.; Hu, W.; et al. Semiconducting π-Conjugated Systems in Field-Effect Transistors: A Material Odyssey of Organic Electronics. *Chem. Rev.* **2012**, *112* (4), 2208–2267. https://doi.org/10.1021/cr100380z.
(293) Dong, H.; Fu, X.; Liu, J.; et al. 25th Anniversary Article: Key Points for High-Mobility Organic Field-Effect Transistors. *Adv. Mater.* **2013**, *25* (43), 6158–6183. https://doi.org/10.1002/adma.201302514.
(294) Hong, G.; Gan, X.; Leonhardt, C.; et al. A Brief History of OLEDs—Emitter Development and Industry Milestones. *Adv. Mater.* **2021**, *33* (9), 2005630. https://doi.org/10.1002/adma.202005630.

(295) Bonaccorso, F.; Sun, Z.; Hasan, T.; et al. Graphene Photonics and Optoelectronics. *Nat. Photonics* **2010**, *4* (9), 611–622. https://doi.org/10.1038/nphoton.2010.186.
(296) Liu, Z.; Fu, S.; Liu, X.; et al. Small Size, Big Impact: Recent Progress in Bottom-Up Synthesized Nanographenes for Optoelectronic and Energy Applications. *Adv. Sci.* **2022**, *9* (19), 2106055. https://doi.org/10.1002/advs.202106055.
(297) Zhi, L.; Müllen, K. A Bottom-up Approach from Molecular Nanographenes to Unconventional Carbon Materials. *J. Mater. Chem.* **2008**, *18* (13), 1472–1484. https://doi.org/10.1039/B717585J.
(298) Khatun, S.; Samanta, S.; Sahoo, S.; et al. Bottom-Up Porous Graphene Synthesis and Its Applications. *Chem. – Eur. J.* **2024**, *30* (68), e202403386. https://doi.org/10.1002/chem.202403386.
(299) Narita, A.; Feng, X.; Müllen, K. Bottom-Up Synthesis of Chemically Precise Graphene Nanoribbons. *Chem. Rec.* **2015**, *15* (1), 295–309. https://doi.org/10.1002/tcr.201402082.
(300) Zhang, Y.; Zhang, L.; Zhou, C. Review of Chemical Vapor Deposition of Graphene and Related Applications. *Acc. Chem. Res.* **2013**, *46* (10), 2329–2339. https://doi.org/10.1021/ar300203n.
(301) Nam, J.; Yang, J.; Zhao, Y.; et al. Chemical Vapor Deposition of Graphene and Its Characterizations and Applications. *Curr. Appl. Phys.* **2024**, *61*, 55–70. https://doi.org/10.1016/j.cap.2024.02.010.
(302) Xin, H.; Li, W. A Review on High Throughput Roll-to-Roll Manufacturing of Chemical Vapor Deposition Graphene. *Appl. Phys. Rev.* **2018**, *5* (3), 031105. https://doi.org/10.1063/1.5035295.
(303) Bubnova, O. A Decade of R2R Graphene Manufacturing. *Nat. Nanotechnol.* **2021**, *16* (10), 1050–1050. https://doi.org/10.1038/s41565-021-00990-5.
(304) Yi, M.; Shen, Z. A Review on Mechanical Exfoliation for the Scalable Production of Graphene. *J. Mater. Chem. A* **2015**, *3* (22), 11700–11715. https://doi.org/10.1039/C5TA00252D.
(305) Liu, N.; Tang, Q.; Huang, B.; et al. Graphene Synthesis: Method, Exfoliation Mechanism and Large-Scale Production. *Crystals* **2022**, *12* (1), 25. https://doi.org/10.3390/cryst12010025.